LRP 500/94 September 1994

GLOBAL MARGINAL STABILITY OF TAEs IN THE PRESENCE OF FAST IONS

L. Villard, S. Brunner and J. Vaclavik

submitted for publication in
Nuclear Fusion

Global Marginal Stability of TAEs in the presence of Fast Ions

L.Villard, S.Brunner and J. Vaclavik

Centre de Recherches en Physique des Plasmas

Association Euratom - Confédération Suisse

Ecole Polytechnique Fédérale de Lausanne

21, av. des Bains – CH-1007 Lausanne/Switzerland

Abstract

The global stability of toroidicity-induced Alfvén eigenmodes (TAEs) in the presence of fast ions in realistic tokamak fusion-grade plasmas is analyzed with a global, perturbative approach. Volume averaged fast particle betas for marginal stability are obtained and analyzed for a wide range of plasma parameters such as the fast ion radial density profile width, the ratio of birth velocity to the Alfvén velocity on axis and the bulk plasma beta. The different stability behaviour of two types of TAEs ('internal' or 'external') is evidenced.

1 Introduction

The destabilization of Toroidicity-Induced Alfvén Eigenmodes (TAEs) [1] by fast particles in tokamak plasmas has been demonstrated both theoretically [2]-[6] and experimentally [7]-[9] . In the context of fusion-oriented research one should be able to predict as accurately as possible the conditions that can lead to such instabilities and to determine whether the region in parameter space where instabilities are avoided is compatible with the operation of a tokamak reactor. The expected density profile of fusion alpha particles in such a device is largely unknown and can only be inferred from theoretical models based on a number of assumptions on transport properties of plasmas yet to be produced. The instability threshold strongly depends on this profile, therefore we must address the question of TAE stability for a wide range of fast particle density profiles and subsequently examine the compatibility with a fusion plasma.

Experiments in which the fast particles were produced by intense NBI heating [7]-[9] have shown that driving TAEs unstable can lead to rapid losses (bursts) of a substantial fraction of the fast particles. Although it is not sure that it would be the case for fusion alphas in a reactor, it is generally admitted that TAE instability should be avoided.

The possibility of exciting TAEs when they are stable is currently investigated at JET. The saddle coils now installed in the machine serve as antennas. The planned experiments aim at determining the spectrum of TAEs and their overall linear damping-growth rate by diagnosing the plasma response. Even in the absence of fast particles these experiments will be helpful in studying the damping mechanisms acting on TAEs.

From local theories [2]-[5] we know that three basic conditions must be met for instability:

1 The birth velocity v_0 of fast particles must exceed the parallel phase velocity v_p of the eigenmode so that the fast particles can resonantly interact with the eigenmode.

2 The fast particle pressure gradient $|dp_f/dr|$ must exceed a given threshold so that the drift frequency $\omega^\star$ is larger than the eigenfrequency ω_0 .

3 The fast particle induced growth-rate, $|\gamma/\omega|_{fast}$, must exceed the sum of all damping rates, $|\gamma/\omega|_{damp}$, due to the presence of the background plasma.

The damping mechanisms contributing to $|\gamma/\omega|_{damp}$ considered in our model are :

a) resonance absorption (sometimes called "continuum damping"), when the TAE eigenfrequency matches a frequency of the Alfvén continuum;

b) electron and ion Landau dampings due to the curvature drift and finite parallel electric field;

c) transit-time magnetic pumping (TTMP) on electrons and ions due to finite parallel magnetic field of the wave (compressibility).

In addition to these dampings the non-perturbative interaction with the kinetic Alfvén wave has been investigated in Ref. [10] . It is not considered in this paper.

Local theories suffer from a number of shortcomings. First, the TAEs are not localized at a given rational $q = (|m| + 1/2)/|n|$ surface. They extend over the whole plasma cross-section, with wavefield components (e.g. the normal electric field) peaking at all such rational surfaces and other components (e.g. the poloidal electric field) having a broader radial dependence [11] . Second, the eigenfrequencies and eigenmode structures depend on global geometrical parameters (shape of the cross-section) and equilibrium profiles (density and q profiles). Third, local theories usually use some kind of expansion in geometrical parameters (a/R_0). A more accurate evaluation is needed in order to model actual and future tokamaks.

In this paper we adopt a global approach similar to that of Ref. [6] . The TAEs are computed globally in true toroidal geometry consistent with an ideal MHD equilibrium. Kinetic effects (damping and driving mechanisms) and fast particles are treated perturbatively. More precisely, we first obtain the global eigenmodes and then use these given eigenmode fields to evaluate the global overall wave-particle power transfer assuming given fast particle density profiles. The marginal stability point is obtained by

scaling the number of fast particles so that the overall power transfer is zero. The wave-particle power transfers (to the electrons, bulk ions and fast ions) are evaluated using the drift-kinetic equations (DKE).

The paper is structured as follows. In the next section, the plasma model in toroidal geometry and the antenna excitation are briefly presented. Then the expressions for the DKE powers are derived for the various species (electrons, bulk ions and fast ions). In section 3 we show the results of our model applied to a wide variety of plasma parameters. In particular, the critical volume-averaged fast particle beta corresponding to marginal stability, $< \beta_f >_{cr}$, is calculated for a wide range of bulk plasma parameters (v_0/v_{A0}, beta, ω/ω_{ci}) and fast particle profile widths ($s_{1/2}$). We discuss the results in section 4 and draw some conclusions in section 5.

2 Model

2.1 Global ideal model for TAE wave fields

We consider ideal MHD axisymmetric equilibria $\vec{B}_0 = T\nabla\varphi + \nabla\varphi \times \nabla\psi$ where T is the toroidal flux function, φ is the toroidal angle and the poloidal flux ψ is a solution of the Grad-Shafranov equation obtained with the bicubic finite element code CHEASE [12] . The plasma is modelled as a cold, current-carrying plasma [13] neglecting electron inertia. In the limit $\omega/\omega_{ci} \rightarrow 0$ it is equivalent to ideal MHD setting the adiabaticity index to zero. The linearized equations for the electric wave field are written in the variational form :

$$\int_{V_p} \left\{ \left| \nabla\times \vec{E} - \vec{J}\, E_b \right|^2 - 2\, \vec{J}\cdot\nabla_{\|}\, \vec{e}_n\, |E_b|^2 - \frac{\omega^2}{c^2}\, \vec{E}^{\star} \cdot \begin{pmatrix} \epsilon_{nn} & \epsilon_{nb} \\ \epsilon_{bn} & \epsilon_{bb} \end{pmatrix} \cdot \vec{E} \right\} d^3x + \int_{V_v} \left| \nabla\times \vec{E} \right|^2 d^3x = 0 \qquad (1)$$

where $\vec{e}_n = \nabla\psi/|\nabla\psi|$, $\vec{e}_{\|} = \vec{B}_0/B_0$, $\vec{e}_b = \vec{e}_{\|} \times \vec{e}_n$, $\vec{J} = (\mu_0\, \vec{j}_0 \times \vec{e}_n)/B_0$, $\vec{j}_0$ is the equilibrium current, V_p is the plasma volume and

$$\epsilon_{nn} = \epsilon_{bb} = \frac{c^2}{v_A^2} \sum_i \frac{f_i}{1 - (\frac{\omega}{\omega_{ci}})^2},$$

$$\epsilon_{nb} = \epsilon_{bn}^* = i \frac{c^2}{v_A^2} \sum_i \frac{f_i \omega / \omega_{ci}}{1 - (\frac{\omega}{\omega_{ci}})^2},$$

$$f_i = \frac{n_i m_i}{\sum_j n_j m_j}. \tag{2}$$

The plasma is surrounded by a vacuum region V_v enclosed by a perfectly conducting wall. In the vacuum region an antenna is modelled by an infinitely thin sheet $D(\vec{x})$ on which currents $\vec{j_a}$ of given frequency ω and toroidal mode number n are prescribed :

$$\vec{j_a} = \delta(D) \nabla D \times \nabla \alpha \tag{3}$$

$$\alpha = \sum_n \alpha_n(\theta) \exp i(n\varphi - \omega t) \tag{4}$$

where θ is the poloidal angle. The coefficients α_n are obtained from the Fourier series decomposition of the actual antenna currents. In this paper we consider the top saddle coil antennas that are installed in JET. Different phasings of the saddle coil currents give different toroidal Fourier spectra α_n. It is thus possible to select the desired mode number n (mainly $n = 1$ or $n = 2$).

Special care must be taken because of the existence of the Alfvén continuous spectrum. First, the solutions of Eq.(1) are singular at the magnetic surfaces where the antenna frequency matches that of a continuum. Consequently the wave is resonantly absorbed there, a process sometimes called "continuum damping". We solve the problem by adding a small imaginary part to the dielectric tensor in Eq.(1): ω is replaced by $\omega(1 + i\nu)$, with $\nu > 0$ to ensure causality. The operator in Eq.(1) is now regular but has lost its hermiticity. The limit $\nu \to 0$ is extrapolated from the numerical results of the LION code and gives a finite damping rate if the wave frequency is in the Alfvén continuum. Second, the discretization scheme must avoid spectral pollution. The use of hybrid elements in the LION code ensures that [11], [13] .

The variational form (1) is written in toroidal axisymmetric geometry using a toroidal magnetic coordinate system (ψ, χ, φ) where χ is a general poloidal coordinate, and discretized with finite hybrid elements in the plasma domain. The vacuum, including the

antenna, is solved with a Green's function technique. The LION code computes the wavefield solution of Eq.(1) and the total absorbed power P for given antenna frequencies ω. A global mode shows as a peak on $P(\omega)$ [11] .

We know from kinetic theory in 1-D [14] that the inclusion of finite Larmor radius effects (FLR) usually does not modify the overall plasma power absorption but drastically changes the wavefields near the former Alfvén resonances : mode conversion to the Kinetic Alfvén Wave (KAW) or to the Surface Quasi-Electrostatic Wave (SQEW) takes place. Therefore this paper is concerned with TAEs that have no continuum damping. Such cases arise when the profile of $1/q\sqrt{\rho}$ is rather flat (q is the safety factor and ρ is the mass density) thus aligning the $q = (|m| + 1/2)/|n|$ gaps. Continuum damping of low n modes was extensively studied in Ref [11] for a wide variety of shapes and profiles. High n cases were analytically studied in Refs [15], [16] . Only for cases where the profile $1/q\sqrt{\rho}$ is sufficiently peaked or hollow do the continuum gaps not overlap and one is sure to have continuum damping. Otherwise we can have TAEs "threading" the gaps and thus exactly zero continuum damping. It is safer to examine these cases since one cannot be sure to exclude them in a reactor (neither the density nor the q profile are easily controllable).

2.2 Global kinetic model for the wave-particle power transfers

The evolution equation used for the plasma species is the Drift Kinetic Equation (DKE)

$$\frac{Df}{Dt} = \left[\frac{\partial}{\partial t} + \vec{v_g} \cdot \frac{\partial}{\partial \vec{X}} + \frac{d\epsilon}{dt}\frac{\partial}{\partial \epsilon} + \frac{d\mu}{dt}\frac{\partial}{\partial \mu}\right] f(\vec{X}, \epsilon, \mu, t) = 0, \tag{5}$$

where $\vec{X}$ is the guiding center, $\epsilon = \frac{1}{2}(v_{\|}^2 + v_{\perp}^2)$, $\mu = v_{\perp}^2/2B_0$, $\vec{v_g} = v_{\|}\ \vec{e}_B + \vec{v_E} + \vec{v_d}$, $\vec{v_E} = \vec{E} \times (\vec{B_0} + \vec{B})/B^2$,

$\vec{v_d} = (m/qB)\ \vec{e}_B \times \left(v_{\perp}^2/2 + v_{\|}^2\right) \nabla \ln B$, $B = \mid \vec{B_0} + \vec{B} \mid$ the total magnetic field, $(\vec{E}, \vec{B})$ the perturbing electromagnetic fields and $\vec{e}_B = (\vec{B_0} + \vec{B})/B$.

Equation (5) is first solved to obtain a stationary distribution function. To lowest

order in the Larmor radius expansion one obtains

$$F = F(\psi, \epsilon, \mu). \tag{6}$$

In particular for electrons and bulk ions a local Maxwellian distribution is chosen

$$F = \frac{N(\psi)}{(\pi v_{th}^2(\psi))^{3/2}} \exp\left(-2\frac{\epsilon}{v_{th}^2(\psi)}\right), \tag{7}$$

with density N and thermal velocity squared $v_{th}^2 = 2T/m$. For the fast particles a slowing-down distribution is assumed [17]

$$F = N(\psi)\frac{C(\psi)}{v^3 + v_c^3(\psi)} H(v_0 - v), \tag{8}$$

$$v_c = \left(3\sqrt{\pi}\frac{m_f + m_i}{m_f m_i} m_e\right)^{1/3} \left(\frac{T_e}{m_e}\right)^{1/2}, \tag{9}$$

$$C = \frac{3}{4\pi \ln\left[\left(\frac{v_0}{v_c}\right)^3 + 1\right]}, \tag{10}$$

where H is the Heaviside function and v_0 the birth velocity of the fast particles ($v_0 = 1.3 \cdot 10^7 m/s$ for fusion alphas).

The linearized DKE is then solved to obtain the fluctuating part of the distribution function in terms of the EM fields

$$\left(\frac{\partial}{\partial t} + \vec{v}_{g0} \cdot \frac{\partial}{\partial \vec{X}}\right) \tilde{f} = -\left(\tilde{\vec{v}}_g \cdot \frac{\partial}{\partial \vec{X}} + \frac{\tilde{d\epsilon}}{dt}\frac{\partial}{\partial \epsilon}\right) F, \tag{11}$$

where

$$\vec{v}_{g0} = v_{\|}\,\vec{e}_{\|} + \vec{v}_{d0}, \tag{12}$$

$$\tilde{\vec{v}}_g = v_{\|}\frac{\vec{B}_\perp}{B_0} + \frac{\vec{E} \times \vec{B}_0}{B_0^2}, \tag{13}$$

$$\frac{\tilde{d\epsilon}}{dt} = \frac{q}{m}\,\vec{v}_{g0} \cdot \vec{E} + \mu\frac{\partial B_{\|}}{\partial t}. \tag{14}$$

As the unperturbed system is homogeneous in time and the toroidal direction, one can consider fluctuating quantities of the form $\exp i[n\varphi - (\omega + i\eta)t]$, where $\eta > 0$ ensures causality. Equation (11) is solved using a perturbation method. The operator $\vec{v}_{d0} \cdot \nabla =$

$\mathcal{O}(\varepsilon)$, on the left hand side is considered as perturbative. Furthermore, to avoid an integration along the field line, the differential operator $\vec{e}_{\|} \cdot \nabla$, is replaced by its magnetic-surface-averaged value $< \nabla_{\|} >= ik_{\|}$, where

$$k_{\|}^2 = \frac{\oint_{\psi=const} dl \left(|\nabla_{\|} E_n|^2 + |\nabla_{\|} E_b|^2 \right)}{\oint_{\psi=const} dl |\vec{E}|^2}, \tag{15}$$

The integrals in Eq.(15) are evaluated along a closed path in the poloidal plane on a $\psi = const$ surface. Another possibility instead of using Eq. (15) would be to make the rough approximation $\omega^2 = v_A^2 k_{\|}^2$, since TAEs are Alfvén waves. But $k_{\|}$ obtained in this way can be wrong by a factor up to 3. The reason is the "sidebands" created by toroidal coupling: simple models give resonances at one third of the Alfvén speed.

Solving to second order in ε and retaining only the most dominant element among comparable terms leads to

$$\begin{aligned} \tilde{f} \;=\; & \frac{-iq}{m\omega_c \Omega_0} \left\{ \frac{1}{\omega} \left(\Omega_0 E_b - i v_{\|} \nabla_p E_{\|} \right) \nabla_n F \right. \\ & + \left[\omega_c v_{\|} E_{\|} + \left(\frac{v_\perp^2}{2} + v_{\|}^2 \right) \vec{\beta}_\perp \cdot \vec{E} - i\omega \frac{v_\perp^2}{2} B_{\|} \right] \frac{\partial F}{\partial \epsilon} \\ & \left. - i \frac{1}{\omega \omega_c} \left(\frac{v_\perp^2}{2} + v_{\|}^2 \right) (\vec{\beta}_\perp \cdot \nabla) E_b \nabla_n F \right\}, \end{aligned} \tag{16}$$

where $\omega_c = qB_0/m$, $\Omega_0 = \omega + i\eta - k_{\|} v_{\|}$, $\vec{\beta}_\perp = \left(\nabla \times \vec{e}_{\|} \right)_\perp$ and $\nabla_p = (\nabla\varphi \times \nabla\psi)/|\nabla\varphi \times \nabla\psi| \cdot \nabla$.

One can now derive the power absorption formula. The total power exchanged between the particles and the perturbing EM fields averaged over time reads

$$P_{species} = \frac{1}{2} \Re e \int d\Gamma \, \frac{\tilde{d\epsilon}}{dt} \tilde{f}^*_{species}, \qquad d\Gamma = d^3X d^3v. \tag{17}$$

Inserting Eqs (14) and (16) leads to the following relations

$$P_{species} = P^{homo}_{species} + P^{inhomo}_{species}, \tag{18}$$

$$P^{homo} \;=\; \frac{1}{2} \Im m \int d\Gamma \frac{q^2}{m\Omega_0} \left| v_{\|} E_{\|} + \frac{1}{\omega_c} \left(\frac{v_\perp^2}{2} + v_{\|}^2 \right) (\vec{\beta}_\perp \cdot \vec{E}) - i \frac{\omega}{\omega_c} \frac{v_\perp^2}{2} B_{\|} \right|^2 \frac{\partial F}{\partial \epsilon}, \tag{19}$$

$$P^{inhomo} = -\frac{1}{2}\Re e \int d\Gamma \frac{q^2}{m\omega\omega_c\Omega_0}\left[v_{\|}E_{\|} + \frac{1}{\omega_c}\left(\frac{v_\perp^2}{2}+v_{\|}^2\right)\vec{\beta}_\perp\cdot\vec{E} - i\frac{\omega}{\omega_c}\frac{v_\perp^2}{2}B_{\|}\right]\times \quad (20)$$
$$\left[\frac{1}{\omega_c}\left(\frac{v_\perp^2}{2}+v_{\|}^2\right)(\vec{\beta}_\perp\cdot\nabla)E_b^* + v_{\|}\nabla_p E_{\|}^*\right]\nabla_n F.$$

The resonant denominator can be written as

$$\frac{1}{\Omega_0} = \frac{1}{\omega - k_{\|}v_{\|} + i\eta} = \mathcal{P}\frac{1}{\omega - k_{\|}v_{\|}} - i\pi\frac{1}{|k_{\|}|}\delta\left(v_{\|} - \frac{\omega}{k_{\|}}\right). \quad (21)$$

Globally, only the resonant particles can exchange energy with the EM fields. The principle value in the above relation can therefore be discarded when evaluating the absorbed power.

For a Maxwellian distribution the power reads

$$P^{homo} = \sqrt{\pi}\epsilon_0\int d^3x\frac{\omega_p^2 v_{th}}{4\omega_c^2|k_{\|}|}\exp(-z_0^2)\times \quad (22)$$
$$\left\{\left|2z_0\frac{\omega_c}{v_{th}}E_{\|} + \left(1+2z_0^2\right)\vec{\beta}_\perp\cdot\vec{E} - i\omega B_{\|}\right|^2 + \left|\vec{\beta}_\perp\cdot\vec{E} - i\omega B_{\|}\right|^2\right\},$$

$$P^{inhomo} = \sqrt{\pi}\epsilon_0\Im m\int d^3x\nabla'_n\frac{\omega_p^2 v_{th}^3}{8\omega\omega_c^3|k_{\|}|}\exp(-z_0^2)\left\{\left[2z_0\frac{\omega_c}{v_{th}}E_{\|} + \left(1+2z_0^2\right)\vec{\beta}_\perp\cdot\vec{E} - i\omega B_{\|}\right]\times\right.$$
$$\left.\left[\left(1+2z_0^2\right)(\vec{\beta}_\perp\cdot\nabla E_b^*) + 2z_0\frac{\omega_c}{v_{th}}\nabla_p E_{\|}^*\right] + \left[\vec{\beta}_\perp\cdot\vec{E} - i\omega B_{\|}\right](\vec{\beta}_\perp\cdot\nabla)E_b^*\right\}, \quad (23)$$

where $\omega_p^2 = Nq^2/m\epsilon_0$, $z_0 = \omega/k_{\|}v_{th}$ and ∇'_n is equivalent to ∇_n except that it operates only on density and temperature. For the slowing-down distribution resonant particles can exist only if the phase velocity is below the birth velocity ($|v_p = \omega/k_{\|}| < v_0$), in that case

$$P^{homo} = \pi^2\epsilon_0\int d^3x\frac{\omega_p^2 C}{|k_{\|}|}\left\{\frac{1}{|v_p|^3+v_c^3}\left|v_p E_{\|} + \frac{1}{\omega_c}v_p^2\vec{\beta}_\perp\cdot\vec{E}\right|^2\right. \quad (24)$$
$$\left. + \frac{2I_0}{\omega_c}\Re e\left(\vec{\beta}_\perp\cdot\vec{E}^* + i\omega B_{\|}^*\right)\left(v_p E_{\|} + \frac{v_p^2}{\omega_c}\vec{\beta}_\perp\cdot\vec{E}\right) + \frac{I_1}{\omega_c^2}\left|\vec{\beta}_\perp\cdot\vec{E} - i\omega B_{\|}\right|^2\right\},$$

$$P^{inhomo} = -\pi^2\epsilon_0\Im m\int d^3x\nabla'_n\frac{\omega_p^2 C}{|k_{\|}|\omega_c}\left\{I_0\left(v_p E_{\|}^* + \frac{v_p^2}{\omega_c}\vec{\beta}_\perp\cdot\vec{E}^*\right)\left(\frac{v_p^2}{\omega\omega_c}(\vec{\beta}_\perp\cdot\nabla)E_b + \frac{\nabla_p E_{\|}}{k_{\|}}\right)\right.$$
$$+\frac{I_1}{2\omega_c}\left[\left(\vec{\beta}_\perp\cdot\vec{E}^* + i\omega B_{\|}^*\right)\left(\frac{v_p^2}{\omega\omega_c}(\vec{\beta}_\perp\cdot\nabla)E_b + \frac{\nabla_p E_{\|}}{k_{\|}}\right)\right. \quad (25)$$
$$\left.\left.+\frac{1}{\omega}(\vec{\beta}_\perp\cdot\nabla)E_b\left(v_p E_{\|}^* + \frac{v_p^2}{\omega_c}\vec{\beta}_\perp\cdot\vec{E}^*\right)\right] + \frac{I_2}{4\omega\omega_c^2}(\vec{\beta}_\perp\cdot\nabla)E_b\left(\vec{\beta}_\perp\cdot\vec{E}^* + i\omega B_{\|}^*\right)\right\},$$

$$\text{where} \quad I_n = \int_{|v_p|}^{v_0} dv \frac{v\left(v^2 - v_p^2\right)^n}{v^3 + v_c^3}. \tag{26}$$

The EM fields are calculated from an ideal model (see Section 2.1) in which $E_{||}$ is approximated by zero. Therefore $E_{||}$ must be obtained from a more general model. The starting point is the quasi-neutrality condition

$$\tilde{N}_e = \tilde{N}_i \,. \tag{27}$$

As the thermal velocity of the electrons can be comparable to the phase velocity ($v_{the} \sim |v_p|$), it is reasonable to evaluate the dominant term of $\tilde{N}_e$ using a kinetic model. For this reason $\tilde{f}_{electron}$ is integrated over velocity and leads to

$$\tilde{N}_e = 2i\frac{eN_e}{m_e\omega\omega_{ce}}\left[\frac{\omega\omega_{ce}}{k_{||}v_{the}^2}(1-Z)E_{||} - \frac{1}{2}Z\left(\vec{\beta}_\perp \cdot \vec{E}_\perp - i\omega B_{||}\right) + \left(\frac{\omega}{k_{||}v_{the}}\right)^2 (1-Z)\,\vec{\beta}_\perp \cdot \vec{E}\right], \tag{28}$$

where $Z \equiv Z\left(\frac{\omega}{|k_{||}|v_{the}}\right)$ is the plasma dispersion function [18] . However, to evaluate $\tilde{N}_i$ one can use a cold fluid model for the ions as $v_{thi} \ll |v_p|$. Due to their relatively large mass, the ions dominate the motion perpendicular to the magnetostatic field. Solving the equation of motion in the perpendicular plane, one obtains for low frequencies $\omega \ll \omega_{ci}$

$$\vec{v} = \frac{e}{m_i\omega_{ci}}\left[\vec{E}_\perp \times \vec{e}_{||} - i\frac{\omega}{\omega_{ci}}\vec{E}_\perp\right], \tag{29}$$

and using the equation of continuity for the ion density gives

$$\tilde{N}_i = -\frac{eN_i}{m_i\omega_{ci}^2}\left[\nabla\cdot\vec{E}_\perp - 2i\frac{\omega_{ci}}{\omega}\vec{\beta}_\perp \cdot \vec{E}_\perp - \omega_{ci}B_{||}\right]. \tag{30}$$

Inserting these density relations in the quasi-neutrality condition leads to

$$E_{||} = -\frac{k_{||}v_{the}^2}{2\omega\omega_{ce}}\left\{\frac{1}{1-Z}\left(i\frac{\omega}{\omega_{ci}}\nabla\cdot\vec{E}_\perp + \vec{\beta}_\perp\cdot\vec{E}_\perp\right) + \left[1 + 2\left(\frac{\omega}{k_{||}v_{the}}\right)^2\right]\vec{\beta}_\perp\cdot\vec{E}_\perp - i\omega B_{||}\right\}. \tag{31}$$

Finally, using the above expression in the power relation for electrons and ions gives

$$P^{homo} = \sqrt{\pi}\epsilon_0 \int d^3x \frac{\omega_p^2 v_{th}}{4\omega_c^2|k_{||}|} \exp -z_0^2 \times \left(|a_{species}|^2 + \left|\vec{\beta}_\perp\cdot\vec{E} - i\omega B_{||}\right|^2\right), \tag{32}$$

$$a_{electron} = \frac{1}{1-Z}\left(i\frac{\omega}{\omega_{ci}}\nabla\cdot\vec{E}_\perp + \vec{\beta}_\perp\cdot\vec{E}_\perp\right), \tag{33}$$

$$\begin{aligned} a_{ion} &= \frac{T_e}{T_i}\frac{1}{1-Z}\left(i\frac{\omega}{\omega_{ci}}\nabla\cdot\vec{E}_\perp + \vec{\beta}_\perp\cdot\vec{E}_\perp\right) - i\omega\left(1+\frac{T_e}{T_i}\right)B_\parallel \\ &+ \left[1+\frac{T_e}{T_i}+2\left(\frac{\omega}{k_\parallel v_{thi}}\right)^2\right]\vec{\beta}_\perp\cdot\vec{E}_\perp\,. \end{aligned} \tag{34}$$

P^{inhomo} can be neglected for these species. This is related to the fact that in the frame of the present work $\omega \gg \omega^\star$ for electrons and ions, where $\omega^\star$ is the characteristic frequency of the drift mode. Note that the contributions of $E_\parallel$ to the power absorbed by the ions are proportional to T_e/T_i. As the average kinetic energy of the fast particles is very high as compared with the energy of the electrons, the contributions of $E_\parallel$ to the power absorbed by the fast particles can therefore be neglected. In this way, one can write for the fast particles

$$\begin{aligned} P_f^{homo} &= \pi^2\epsilon_0\int d^3x\frac{\omega_{pf}^2 C}{|k_\parallel|\omega_{cf}^2}\left\{\left[\frac{v_p^4}{|v_p|^3+v_c^3}+2v_p^2 I_0\right]\left|\vec{\beta}_\perp\cdot\vec{E}\right|^2\right. \\ &\left. + 2\omega v_p^2 I_0\Im m\left(B_\parallel\,\vec{\beta}_\perp\cdot\vec{E}^\star\right) + I_1\left|\vec{\beta}_\perp\cdot\vec{E} - i\omega B_\parallel\right|^2\right\}, \end{aligned} \tag{35}$$

$$\begin{aligned} P_f^{inhomo} &= \frac{\pi^2\epsilon_0}{\omega}\Im m\int d^3x\nabla_n'\frac{\omega_{pf}^2 C}{|k_\parallel|\omega_{cf}^3}\left\{\left(v_p^4 I_0 + v_p^2\frac{I_1}{2}\right)\vec{\beta}_\perp\cdot\vec{E}\right. \\ &\left. + \left(v_p^2\frac{I_1}{2}+\frac{I_2}{4}\right)\left(\vec{\beta}_\perp\cdot\vec{E} - i\omega B_\parallel\right)\right\}(\vec{\beta}_\perp\cdot\nabla)E_b^\star. \end{aligned} \tag{36}$$

The expressions (32)-(36) have been written in toroidal axisymmetric geometry and implemented in the LION code.

Marginal stability is reached when the sum of the DKE powers of the different species $P_{species}$ is zero. For a given TAE, a given $n_f(s)$ profile shape and given $T_e(s)$ and $T_i(s)$ profiles ($s=\sqrt{\psi/\psi_s}$ is the minor radius coordinate, where ψ_s is the poloidal flux at the plasma surface), both P_f^{homo} and P_f^{inhomo} are proportional to the number of fast particles, or equivalently to the fast particle central density $n_f(0)$. The procedure to obtain the value $n_f(0)_{crit}$ corresponding to the marginal stability of a given TAE is the following:

P_e, P_i, P_f^{homo} and P_f^{inhomo} are computed for given $T_e(s)$ and $T_i(s)$ and for a given $n_f(s)$ profile shape with an arbitrary value of $n_f(0)$. We have then

$$n_f(0)_{crit} = -\frac{P_e + P_i}{P_f^{homo} + P_f^{inhomo}} n_f(0). \tag{37}$$

From this value of $n_f(0)_{crit}$ and the given profiles $n_f(s)$ and $T_e(s)$ we compute the corresponding critical central fast particle beta $\beta_f(0)_{crit}$ and volume-averaged $< \beta_f >_{crit}$. We note that $n_f(0)_{crit} < 0$ means that the mode is always stable (i.e. stable for any fast particle density). Thus instead of the necessary instability criterion of local theories, $\omega - \omega^* < 0$, we have the necessary global instability criterion $P_f^{homo} + P_f^{inhomo} < 0$.

3 Results

3.1 Excitation of gap modes with JET saddle coils

We consider an up-down asymmetric equilibrium configuration representative of a "single-null" discharge in JET. The parameters are: $a/R_0 = 0.36$, $\kappa = 1.65$, $q_0 = 1.1$, $q_a = 3.34$, $p'(\psi) = 2/3$ of ballooning optimized $p'(\psi)$ profile, $I_p = 5MA$, $< \beta >= 3.9\%$, $\beta_{pol} = 0.78$. In all the equilibria considered in this paper we keep the same shape of cross-section, value of q_0 and $I^*(\psi)$ profile, where I^* is the magnetic-surface-averaged toroidal current density. Different equilibria are obtained by scaling the $p'(\psi)$ profile.

We first evaluate the plasma response to the antenna excitation at various frequencies in the absence of kinetic effects. Fig.1 shows the antenna coupling resistance vs frequency for the case $< \beta >= 3.9\%$ and for two different possible antenna phasings. Note that for standard JET parameters $R_0 = 3m$, $B_0 = 3.45T$, $n_{D0} = 5 \times 10^{19} m^{-3}$ a normalized frequency $R_0\omega/v_{A0}$ of unity corresponds to a frequency $f = 400kHz$. The dotted line corresponds to two top antennas at opposite toroidal locations with opposite phasings, exciting mainly $n = 1$ modes. The continuous line corresponds to all four top antennas with $(+,-,+,-)$ phasings, exciting mainly $n = 2$ modes. Saddle coils excite TAEs in the frequency range $f = 80 - 250kHz$ and EAEs (Ellipticity-Induced Alfvén Eigenmodes) in the frequency range $f = 250 - 500kHz$. The different modes can have very different

couplings and this is due to different eigenmode structures. For example, the $n = 1$ mode labelled "a" in Fig.1 has an "internal" structure (Fig.2a) with a relatively modest wave amplitude at the plasma boundary and therefore a much smaller coupling than the mode labelled "b" which has the structure of an "external" mode shown in Fig.2b with a large wave amplitude throughout the plasma cross-section. We point out another basic difference between these two types of modes. The eigenfrequency of mode "a" is very close to the lower edge of the toroidicity induced gap. The mode "a" is rather insensitive to the position of the vacuum vessel whereas mode "b" is very sensitive to it: its frequency increases with a shorter plasma-wall distance and it does not exist for a wall right on the plasma boundary. The TAEs studied in Refs [1], [3], [6], [19] , being calculated with a fixed boundary, are of the "a" type ("internal").

Before we analyze the consequences of these differences in eigenmode structures on the fast particle destabilization, we point out another interesting difference in behaviour from the point of view of the strictly ideal model. Fig.3 shows the eigenfrequencies of the modes "a" and "b" for a sequence of equilibria with varying pressure. The mode "a" hardly changes its eigenfrequency and always remains just above the lower edge of the continuum gap. The fact that its frequency decreases just reflects the opening of the gap as the Shafranov shift of magnetic surfaces increases. Its coupling from the antennas remains quite small and roughly constant. Mode "b", on the other hand, is very sensitive to variations in the plasma equilibrium. Its frequency decreases strongly with increasing β_{pol}, by a factor 2 for $\beta_{pol} \simeq 2.4$. For $\beta_{pol} \simeq 2.25$ the two modes cross each other and for still higher β_{pol} mode "b" enters the Alfvén continuum. The antenna coupling of mode "b" exhibits a remarkable behaviour: it is linearily proportional to β_{pol} (see Fig.4). This is an effect of the increased Shafranov shift and a stronger variation in B_{0pol} along field lines as the equilibrium pressure is scaled up. The compressibility of the mode (finite $B_{||}$) increases with β_{pol}(see Fig.4). The mode "b" also becomes less torsional: the ratio of amplitudes $E_n/E_\perp$ decreases from 15.4 for $\beta_{pol} = 0.78$ to 4.1 for $\beta_{pol} = 2.14$. Therefore gap modes are "Alfvén modes" only in a loosely speaking sense. One cannot a priori rule

out the effect of TTMP on gap modes. This is why we chose to retain finite $B_{||}$ in our DKE model (see Eqs(32)-(36)). A practical consequence is that it will be hard to see the mode "b" for low β_{pol} values in the antenna excitation experiments. We note also that the frequency decrease with increasing beta has been seen in the DIII-D experiment [20] . The factor 2 decrease that we found is of the same order as reported in Ref. [20] . The authors of Ref. [20] have given another interpretation to this effect and named the high-beta TAE modes Beta-Induced Alfvén Eigenmodes (BAE).

3.2 Stability of TAE modes in the presence of fast ions

In what follows we analyze the $n = 1$ stability of the lowest frequency modes corresponding to modes "a" and "b" in Figs.1-4. From the point of view of the necessary condition for instability $\omega^\star > \omega$, these are the most dangerous modes. Let us first consider the mode "a" (Fig.2(a)) with the parameters $R_0 = 3m$, $n_{D0} = 5 \times 10^{19} m^{-3}$, $B_0 = 3.45T$, $T_{e0} = 10keV$, $T_{i0} = 30keV$, in the presence of fusion alpha particles. We consider fast particle density profiles defined by

$$n_f(s) = n_{f0}(1 - s^2)^{\kappa_f}, \tag{38}$$

and vary the profile peaking by varying κ_f. Moreover, we define the quantity $P(s)$ by the relation

$$P_{species} = \int_0^1 P(s)ds. \tag{39}$$

Fig.5 shows $P(s)$ of the different species, Eqs.(32)- (36), plotted versus s for $\kappa_f = 22$ which gives an alpha particle profile half-width $s_{1/2} = 0.176$. As expected the destabilizing term P_f^{inhomo} peaks around $s = 0.15$ where the alpha particle density gradient is maximal. The fast particle stabilizing term P_f^{homo} shows a similar behaviour. The electron damping, on the other hand, is localized near $s = 0.8$ ($q = 1.5$) where eigenmode gradients are very large (see Fig.2a). The ion damping is maximal near $s \simeq 0.5$. This can be understood from the factor $\exp\{-(\omega/|k_{||}|v_{thi})^2\}$ in P^{homo}. Due to the $k_{||}$ variation with respect to s, the quantity $\omega/|k_{||}|v_{thi}$ is minimal near $s \simeq 0.5$(see Fig.6). This example shows the

importance of determining the overall stability globally. Local stability criteria would give instability if applied near $s = 0.2$ but stability if applied near $q = 1.5$ ($s = 0.8$). The influence of the eigenmode structure on the stability plays a crucial role. First, through the profile of eigenmode wave fields and their gradients (Fig.2). Second, through the profile of $k_{||}$ (Fig.6).

For the same parameters as in Fig.5 (except the fast particle density profile half-width $s_{1/2}$ and the central ion temperature T_{i0} which are varied) we show in Fig.7 the critical volume averaged fast-particle beta for marginal stability, $< \beta_f >_{cr}$, plotted versus the profile half-width $s_{1/2}$ for various central ion temperatures T_{i0}. The stabilizing effect of ion damping is clear for $T_{i0} \geq 20keV$. We note a remarkable behaviour of $< \beta_f >_{cr}$ vs $s_{1/2}$. For $s_{1/2} \tilde{<} 0.35$, flattening the fast particle profile is stabilizing as one can expect. But for $0.35 < s_{1/2} < 0.55$ flattening the fast particle profile actually destabilizes the mode: the reason is that an increasingly large fast particle pressure gradient is present near $s = 0.8$ ($q = 1.5$) where the eigenmode has a large amplitude (Fig.2a). This effect is not small : $< \beta_f >_{cr}$ is about a factor 2 larger for $s_{1/2} = 0.35$ than for $s_{1/2} = 0.65$. This means that about half of the fast particles would be lost if the fast particle profile widens beyond $s_{1/2} = 0.35$. For $s_{1/2} > 0.65$, flattening the fast particle profile is again stabilizing because of the reduced fast particle pressure gradient.

3.3 Dependence on the fast particle profile width $s_{1/2}$, bulk plasma β, v_0/v_{A0} and ω/ω_{ci}

In this section we consider the same sequence of plasma MHD equilibria as before but consider the case where both bulk ions and fast ions are deuterium species. Fast ions birth energy is $75keV$. The temperature and density profiles are chosen as $T_e(s) = T_{e0}(1-s^2)^{1/2}$, $T_i(s) = T_{i0}(1-s^2)^{1/2}$, $n(s) = n_0(1-0.9s^2)^{1/2}$ and $n_f(s) = n_{f0}(1-s^2)^{\kappa_f}$. We keep the ratio T_i/T_e constant at 1.25. Different values of bulk β, v_0/v_{A0} and ω/ω_{ci} are obtained by varying the bulk density n_0, temperatures T_{i0} and T_{e0} and magnetic field

B_0 each over a wide range of values:

$$\begin{aligned} B_0 &= 0.6 - 2.25 \quad T \\ n_0 &= 1.3 - 30 \times 10^{19} \quad m^{-3} \\ T_{i0} &= 0.15 - 12.8 \quad keV \\ T_{e0} &= 0.12 - 10.3 \quad keV \end{aligned}$$

We set the major radius of magnetic axis at $1.8m$. These parameters overlap those of DIII-D TAE excitation experiments with NB injection [8], [9], [20] . We study the fast particle critical beta corresponding to marginal stability of TAE modes "a" and "b" for a range of fast particle profile widths $s_{1/2}$ obtained by varying the coefficient κ_f.

The damping on bulk species depends on the ratios $\omega/|k_{||}|v_{the}$, $\omega/|k_{||}|v_{thi}$ and ω/ω_{ci} (see Eqs.(32)-(34)). The TAE eigenfrequencies ω scale proportionally to the Alfvén velocity on axis v_{A0}, so the ratio $\omega/|k_{||}|v_{the}$ is proportional to $1/\beta_e$,$\omega/|k_{||}|v_{thi}$ is proportional to $1/\beta_i$, and $(\omega/\omega_{ci})^2$ is proportional to $1/n_0$. Thus for given $T_e(s)$, $T_i(s)$, $n(s)$ profile shapes and for a fixed T_{i0}/T_{e0} ratio the damping on bulk ions and electrons of a given TAE depends only on the plasma beta and on the bulk density n_0. The DKE power on fast ions depends on the ratio v_0/v_p through the integrals I_0, I_1 and I_2 in Eqs.(35)(36) and on the profile width $s_{1/2}$ through the parameter κ_f in Eq.(38). For a given TAE mode, v_p scales proportionally to v_{A0}. So the overall global stability properties of a given TAE mode in a plasma with given profile shapes of $T_i(s)$, $T_e(s)$ and $n_i(s)$ and a fixed T_{i0}/T_{e0} ratio are determined by the plasma beta, the ratio ω/ω_{ci} (bulk density n_0), the fast particle profile width $s_{1/2}$ and the ratio v_0/v_{A0}. The global stability of TAEs depends also on the eigenmode wavefield structure as was illustrated in the previous section.

Before studying the stability of TAE modes in the presence of fast particles, we have analyzed the DKE powers on electrons and bulk ions. For a given TAE mode and a fixed plasma beta, we found that P_e depends linearly on $(\omega/\omega_{ci})^2$, for any combination of T_{e0}, n_{e0} and B_0 giving the same beta. So P_e depends on β_e and n_0. On the other hand we have found that P_i depends very weakly on ω/ω_{ci} and can be considered as a function of

β_i only.

We show in Fig.8 the critical volume-averaged fast particle beta, $< \beta_f >_{cr}$, plotted as a function of the fast particle profile half-width $s_{1/2}$, for various ratios of the birth velocity to the Alfvén velocity on axis, v_0/v_{A0}. All data in Fig.8 has been calculated with the same equilibrium plasma beta of 3% and for the "internal" $n = 1$ TAE mode ("a" in Figs 1-3). The ratio v_0/v_{A0} was varied by changing the density n_0 and the temperature T_{i0}, T_{e0} as $1/n_0$, keeping B_0 constant, so that β is constant. As in Fig.7, we have a remarkable behaviour of $< \beta_f >_{cr}$ vs $s_{1/2}$. For $s \lesssim 0.35$ widening the fast particle profile is stabilizing because the fast particle pressure gradient is decreased. But for $s \gtrsim 0.35$ the opposite is true: although the fast particle pressure gradient term is decreasing, the destabilization comes from the increasingly large fast ion pressure gradient near the $q = 1.5$ surface where the TAE wave field and its gradient are large (see Fig.2a). For $s_{1/2}$ near 0.6 the two effects balance about each other and for still larger $s_{1/2}$ values the stabilizing effect of flattening the fast particle profile dominates.

We note that for $v_0/v_{A0} \gtrsim 1$ the $< \beta_f >_{cr}$ is lower for $s_{1/2} = 0.7$ (which corresponds to $n_f(s) = n_{f0}(1 - s^2)$) than for $s_{1/2} = 0.35$ (which corresponds to $n_f(s) = n_{f0}(1 - s^2)^6$). This particular behaviour is a consequence of the TAE mode structure. By no means could a local theory predict such a behaviour. It may have implications on the evolution of the fast particle contents in the discharge: if this mode is close to marginal stability and if $s_{1/2}$ goes beyond 0.35, the loss of fast particles, flattening the profile, would make the mode more unstable, so that fast particles would continue to be expelled until $s_{1/2}$ is about 0.6. Only then can the fast particle profile build up again in the center. But in the meantime, we see from Fig.8 that about half of the energy content of fast particles would have been lost. Note that this may be related to the "bursts" of expelled fast particles sometimes seen in the experiments [7]-[9] . Of course a nonlinear study is needed to properly predict the time behaviour of fast particles [21] .

For the same parameters as in Fig.8, we show in Fig.9 the behaviour of $< \beta_f >_{cr}$ versus the ratio v_0/v_{A0} for different fast particle density profile widths $s_{1/2}$. For a given

$s_{1/2}$, $< \beta_f >_{cr}$ is a monotonically decreasing function of v_0/v_{A0}. We note that this TAE mode can become unstable even for values of v_0/v_{A0} as small as about 0.6. This is due to the behaviour of $|k_{||}|$ of the mode, which is not exactly ω/v_A, but is lower in this case due to the presence of "sidebands" in the poloidal Fourier mode numbers m: the poloidal Fourier decomposition of the eigenmode wavefield shows actually a rather broad m spectrum, due to the small aspect ratio, the elongation and shape of this configuration.

For a given fast ion profile width $s_{1/2} = 0.4$ and plasmas of different beta values we show in Fig.10 the $< \beta_f >_{cr}$ versus v_0/v_{A0}, for the same parameters as in Fig.9 except the plasma beta. For all β values $< \beta_f >_{cr}$ is a decreasing function of v_0/v_{A0}. For v_0/v_{A0} close to 0.7, little effect of beta on $< \beta_f >_{cr}$ is seen: in this region of parameter space, the stability is determined mainly by the competition between P_f^{inhomo} and P_f^{homo} , and the stability diagram corresponds in fact to a threshold in v_0/v_{A0} of about 0.7. For larger values of v_0/v_{A0}, increasing beta is always stabilizing through enhanced electron and ion Landau dampings. We note that for $v_0/v_{A0} < 2$ and $\beta = 1\%$ we have $< \beta_f >_{cr} > 0.4\%$, which is indeed larger than the estimated $< \beta_\alpha >$ in TFTR D-T experiments [22] in which no sign of TAE activity was reported.

In the next three figures (11,12 and 13) we show the corresponding results of Figs 8,9,10 but for the $n = 1$ "external" mode ("b"). In Fig.11 the values of $< \beta_f >_{cr}$ are plotted versus the fast profile width $s_{1/2}$, for a given bulk beta of 3% and for various values of v_0/v_{A0} obtained by varying n_{i0} and T_{e0}, T_{i0} as $1/n_0$. For $s_{1/2} < 0.4$, $< \beta_f >_{cr}$ is increasing with $s_{1/2}$ as the fast ion gradient decreases. For $s_{1/2} \tilde{>} 0.4$ the behaviour of $< \beta_f >_{cr}$ versus $s_{1/2}$ depends dramatically on the value of v_0/v_{A0}. For $v_0/v_{A0} \tilde{<} 1.5$, $< \beta_f >_{cr}$ monotonically increases with $s_{1/2}$. But for $v_0/v_{A0} \tilde{>} 1.5$ the opposite is true. This particular behaviour, which is quite different from that of the "internal" $n = 1$ mode (Fig.8), must be related to the global eigenmode wavefield structure, which is rather flat in the center but has maximum amplitude in the outer region(Fig.2b). For v_0/v_{A0} above 1.5, the ratio v_0/v_p in the outer region is above unity for this mode: fast particles, if present there, will be destabilizing. This is the reason for the decrease in $< \beta_f >_{cr}$ versus

$s_{1/2}$ for $s_{1/2} \tilde{>} 0.4$. For v_0/v_{A0} below 1.5 the ratio v_0/v_p is below unity in the outer region where the mode amplitude is large and therefore no destabilization occurs by flattening the fast particle profile.

In Fig.12 $< \beta_f >_{cr}$ is represented versus v_0/v_{A0} for various profile widths $s_{1/2}$. For this bulk beta value of 3%, $< \beta_f >_{cr}$ is decreasing with v_0/v_{A0} in all cases. We note that this mode can be destabilized for values of v_0/v_{A0} as low as about 0.8.

The behaviour of $< \beta_f >_{cr}$ versus v_0/v_{A0} for this "external" $n = 1$ mode has a remarkable dependence on plasma beta, which is shown in Fig.13. For large v_0/v_{A0} the TAE is stabilized when beta increases, due to enhanced electron and ion Landau damping. On the other hand, increasing beta is destabilizing for small v_0/v_{A0}: the minimum v_0/v_{A0} for instability goes from 1 for $\beta = 1\%$ down to 0.7 for $\beta = 5.5\%$. Increasing beta is lowering the eigenfrequency of this mode (see Fig.3). Consequently the parallel phase velocity is decreasing and more fast particles can destabilize the mode. Therefore the threshold in v_0/v_{A0} is going down with increasing beta for this mode. This is not the case for mode "a" (see Fig.10) because it is rather insensitive to beta (see Fig.3).

We now turn to the stability analysis of $n = 2$ and $n = 3$ TAEs. The wavefield of a $n = 2$ TAE is shown in Fig.14. It corresponds to the peak labelled 'C' in Fig.1. It has the structure of en external mode having a wavefield extending over the whole cross-section, with relative maxima at rational surfaces $q = (|m| + 1/2)/|n|$. The main differences with the $n = 1$ external TAE wavefield are the smaller amplitude near the magnetic axis and a poloidal structure exhibiting larger poloidal mode numbers m. The stability behaviour of this $n = 2$ TAE is shown in Figs. 15 and 16. For v_0/v_{A0} near unity the $< \beta_f >_{cr}$ instability threshold ranges from 0.3% to 1%. As for the $n = 1$ external TAE, we note a monotonic dependence of $< \beta_f >_{cr}$ on $s_{1/2}$ for $v_0/v_{A0} < 1.5$ and a drop of $< \beta_f >_{cr}$ for $v_0/v_{A0} < 1.5$ which is due to the large mode amplitude near the edge: note that $s_{1/2} = 0.71$ corresponds to a parabolic fast ion density profile that has maximal gradient at the plasma edge, which is probably not very realistic. A comparison of Fig.15 ($n = 2$) with Fig.11 ($n = 1$ external) shows that the $n = 1$ mode is more unstable than the $n = 2$

mode only for very peaked fast ion density profiles ($s_{1/2} \lesssim 0.3$). This is due to the larger amplitude of the $n = 1$ mode near the magnetic axis: having a large fast ion density gradient there is therefore more destabilizing than for the $n = 2$ mode. As can be seen from Fig.16 the $n = 2$ TAE can become unstable for v_0/v_{A0} as small as 0.6.

The wavefield of a $n = 3$ TAE is shown in Fig.17. This mode is also of the external type. It is as global as the $n = 1$ and $n = 2$ modes: a comparison of Figs. 2(b), 14 and 17 shows that there is no increase in the 'localization' of the eigenmode with increasing n. The $n = 3$ TAE wavefield is practically zero at the magnetic axis, and this has consequences on the stability behaviour shown in Figs.18 and 19: for very peaked fast ion density profiles the large fast ion density gradient is located where the mode amplitude is small. As a result $< \beta_f >_{cr}$ is nearly constant for $0.18 < s_{1/2} < 0.4$. For $v_0/v_{A0} = 1$, $< \beta_f >_{cr}$ ranges from 0.4% to 1.3%. We note that the $n = 3$ instability threshold is very close to that of the $n = 2$. This may explain why TAEs with different toroidal wavenumbers are simultaneously excited [9].

4 Discussion

Our model is based on a certain number of assumptions and simplifications that we can summarize as follows. First, the kinetic effects have been considered as a small perturbation of the ideal TAE wave fields. The dissipative contributions of the kinetic effects have been taken into account (damping and drive) but not their effect on dispersion. Since those cannot be considered small in the vicinity of Alfvén resonant surfaces, we have restricted our analysis to cases where TAEs have no Alfvén resonances and thus no continuum damping (in other words, no conversion to KAW or SQEW). In this sense our results can be considered as a pessimistic evaluation of the TAE stability especially for low n modes for which continuum damping is most efficient, since it goes as $n^{-3/2}$ for high n [15], [16] . Second, we have neglected trapped particle and finite drift orbit width effects.

On the other hand, we have solved the problem globally in exact toroidal geometry

and we have shown that this approach can give very different results from those of local models (see e.g.Fig.5). The global eigenmode wavefield structure is an important factor determining the instability threshold. In particular, $< \beta_f >_{cr}$ can be a non-monotonic function of the fast particle density profile width and in many cases flattening the fast particle density profile is destabilizing (Figs 7, 8, 11, 15 and 18). This may have consequences on the existence of bursts of expelled fast particles that are seen in some experiments [7]-[9] .

We have identified and studied two types of TAEs: type "a" (internal) and type "b" (external) having different wave fields (Fig.2) and therefore different stability properties (Figs.8-13). They behave differently with respect to equilibrium plasma parameters, in particular the plasma β. They also couple differently to an antenna (Fig.1): type "a" TAEs couple rather weakly and independently of β, wheras type "b" TAEs couple better and approximately proportionally to β due to the increased compressibility of the mode (Fig.4).

Finite β affects the TAEs and their stability in the following way. Increasing β is always stabilizing type "a" TAEs in strengthening the damping on bulk species (Fig.10). The effects on type "b" TAEs are more complex. The real part of the eigenfrequency decreases with β (Fig.3). This was seen in the DIII-D experiment [20] and already computed for circular cross-sections [11] . Therefore the parallel phase velocity decreases and more fast particles can resonantly interact with the wave and destabilize it. This destabilizing effect competes with the increased damping on bulk species with increasing β and the final result can be summarized as a decrease in the v_0/v_{A0} instability threshold ($v_0/v_{A0} < 1$) and an increase in $< \beta_f >_{cr}$ for v_0/v_{A0} above unity (Fig.13). We note that the v_0/v_{A0} instability threshold below unity (~ 0.6) is in a good agreement with the DIII-D experiment [9] .

The parameters determining the TAE stability are: v_0/v_{A0}, β and n_0, for the damping on bulk species and, in addition, β_f and $s_{1/2}$ for the drive and damping on fast ions. Although the computations presented in this paper were not made with the intent to

analyze a particular experimental shot, we can give some clues as to how our results should be interpreted so that a comparison with experiment can be made. The time evolution of a discharge should be analyzed as a motion in the 5-dimensional parameter space v_0/v_{A0}, β, n_0, β_f, $s_{1/2}$ (note that additional parameters such as plasma shape, current, density and temperature profiles could also be important but were not varied in this paper). The instability thresholds calculated with our model can be viewed as $< \beta_f >_{cr}$ surfaces function of the four other parameters. Instability occurs when the trajectory of the discharge crosses a $< \beta_f >_{cr}$ surface. Let us consider the example of NB injection and, for the sake of simplicity, let us assume that $s_{1/2}$ is constant. As NBI is switched on, there is a β_f increase, a bulk β increase and quite frequently a density increase, which implies an increase in v_0/v_{A0} if B_0 is kept constant. Let us consider the stability of type "b" TAE (Fig.13). The trajectory of the shot projected on Fig.13 is then a line going in the upward right side direction. But β is increasing, which means that if v_0/v_{A0} is of order unity or even lower and β_f of the order of 1%, the instability threshold will be crossed for any value of β. We note that these values of β_f and v_0/v_{A0} are in close agreement with the DIII-D experiments (see Fig.10 of Ref. [9]). There may be other shots that evolve in such a way that the bulk β increases fast enough so that the shot trajectory remains below $< \beta_f >_{cr}$ at any time; this can happen even if v_0/v_{A0} is much larger than 1. Although this is also in qualitative agreement with experiment [9] , a more careful comparison should be made, including the study of higher n modes. With increasing n, the radial and poloidal eigenmode structure becomes more and more difficult to resolve numerically. We are therefore restricted to the study of low n modes.

Besides a comparison of the mode frequencies and instability thresholds with experiment, another check would be to compare the wavefields in vacuum with those measured with magnetic probes. The analysis is complicated by the fact that very often several n's are seen simultaneously [9]. One could have expected to see the most unstable modes only. This indicates that the different modes observed are in fact one mode having several n's coupled by a break of axisymmetry. This break could come either from a non-linearity

when the mode amplitude is large, or from error fields and ripple. We note that the eigenfrequencies of different n's can be very close to each other (see e.g. modes labelled 'b' ($n = 1$) and 'C' ($n = 2$) in Fig.1). This implies that a small amount of non-axisymmetry can substantially couple different n's, resulting in a change in eigenmode structure and eigenfrequency.

5 Conclusions

We have developed a hybrid fluid kinetic model for the quantitative prediction of the global linear stability of low n TAEs in the presence of a fast ion population. We have applied this model to a wide variety of cases in order to study the dependence of the TAE stability on a certain number of parameters which were varied over a wide range. The critical volume-averaged fast ion beta corresponding to marginal stability, $< \beta_f >_{cr}$, was studied versus the four parameters: v_0/v_{A0}, β, n_0 and $s_{1/2}$. Typical values of $< \beta_f >_{cr}$ are, for v_0/v_{A0} near unity, in the range 0.3% to 2%, which is in rather good overall agreement with the DIII-D experiment [9] . For $v_0/v_{A0} = 1.5$, the $< \beta_f >_{cr}$ instability threshold is around 0.3%. It can become smaller than 0.1% only for very peaked fast ion density profiles or for very low bulk plasma beta. The finite β effects on type "b" (external) TAEs are a strong decrease in real eigenfrequency, a decrease in the v_0/v_{A0} threshold and a stabilizing effect for v_0/v_{A0} above unity.

We have shown that a global stability analysis is a necessity: the fast ion drive, damping on electrons, damping on bulk ions and damping on fast ions take place at different radial positions. The TAE wave fields extend over the whole plasma cross-section. There is no mode localization, even with increasing n. This fact complicates the analysis of experiments in which there is a toroidal velocity shear: one does not know what the Doppler shift is.

Our results are in agreement with experiments so far. More work is necessary to further assess the validity and applicability of our model, in particular a more detailed case-by-case analysis of some experiments. The saddle coil experiment at JET will also

provide interesting material for a comparison with theory.

There may be positive aspects to the Alfvén wave destabilization by fast particles. The presence of wave fields modifies the way fusion alpha particles give their energy to bulk species: for example, the alpha energy can be transfered directly to ions (see e.g. Fig.5) in a non-classical way, by collisionless mechanisms. One possible scenario could be to operate in a situation where a TAE (or another mode such as the GAE) is unstable but with a saturated amplitude small enough not to destroy alpha particle confinement. Another possibility would be to operate when TAEs and other modes are stable and excite a TAE or a GAE with an antenna. If the mode is close to marginal stability, a large power transfer between fast ions and bulk species can take place even with a moderate antenna power.

Acknowledgments

This work was partly supported by the Swiss National Science Foundation. We thank Dr. H. Lütjens for the equilibrium code CHEASE and Drs A. D. Turnbull and W. W. Heidbrink for interesting discussions.

References

[1] CHENG, C.Z., CHANCE, M.S., Phys.Fluids **29** (1986) 3695.

[2] FU, G.Y., VAN DAM, J.W., Phys.Fluids B **1** (1989) 1949.

[3] CHENG, C.Z., Phys.Fluids B **3** (1991) 2463.

[4] BELIKOV, V.S., KOLESNICHENKO, YA.I., SILIVRA, D.A., Nucl.Fusion **32** (1992) 1399.

[5] BIGLARI, H., ZONCA, F., CHEN, L., Phys.Fluids B **4** (1992) 2385.

[6] FU, G.Y., CHENG, C.Z., WONG, K.L., Phys.Fluids B **5** (1993) 4040.

[7] WONG, K.L., FONCK, R.J., PAUL, S.F., ET AL., Phys.Rev.Lett. **66** (1991) 1874.

[8] HEIDBRINK, W.W., STRAIT, E.J., DOYLE, E., ET AL., Nucl.Fusion **31** (1991) 1635.

[9] STRAIT, E.J., HEIDBRINK, W.W., TURNBULL, A.D., CHU, M.S., DUONG, H.H., Nucl.Fusion **33** (1993) 1849.

[10] METT, R.R., MAHAJAN, S.M., Phys.Fluids B **4** (1992) 2885.

[11] VILLARD, L., FU, G.Y., Nucl.Fusion **32** (1992) 1695.

[12] LÜTJENS, H., BONDESON, A., ROY, A., Comput.Phys.Commun. **69** (1992) 287.

[13] VILLARD, L., APPERT, K., GRUBER, R., VACLAVIK, J., Comput.Phys.Rep. **4** (1986) 95.

[14] APPERT, K., HELLSTEN, T., LUTJENS, H., SAUTER, O., VACLAVIK, J., VILLARD, L., in Plasma Physics (Proc. 7th Int.Conf.Kiev, 1987), Invited papers, Vol.2, World Scientific, Singapore (1987) 1230.

[15] ROSENBLUTH, M.N., BERK, H.L., VAN DAM, J.W., LINDBERG, D.M., Phys.Rev.Lett. **68** (1992) 596.

[16] ZONCA, F., CHEN, L., Phys.Rev.Lett. **68** (1992) 592.

[17] KOCH, R., Phys.Lett. A **157**, (1991) 399.

[18] SHAFRANOV, V.D., in Reviews of Plasma Physics, edited by M.A.Leontovich (Consultants Bureau, New York, 1967) Vol.3.

[19] POEDTS, S., KERNER, W., GOEDBLOED, J.P., KEEGAN, B., HUYSMANS, G.T.A., SHWARTZ, E., Plasma Phys.Control.Fusion **34** (1992) 1397.

[20] HEIDBRINK, W.W., STRAIT, E.J., CHU, M.S., TURNBULL, A.D., Phys.Rev.Lett. **71** (1993) 855.

[21] BERK, H.L., BREIZMAN, B.N., YE, H., Phys.Rev.Lett. **68** (1992) 3563.

[22] STRACHAN, J.D., ADLER, H., ALLING, P., ET AL., Phys.Rev.Lett. **72** (1994) 3526.

Figures

Fig.1. JET saddle coils resistive coupling versus frequency for two possible antenna phasings: two top antennas with (+,-) phasings (dotted line) and four top antennas with (+,-,+,-) phasings. The labels a,b,c,d,e correspond to $n = 1$ modes and A,B,C,D,E,F,G to $n = 2$ modes. The plasma parameters are $R_0 = 3m$, $B_0 = 3.45T$, $n_{D0} = 5 \times 10^{19} m^{-3}$, $\nu = 10^{-2}$, $q_0 = 1.1$, $q_a = 3.34$, $I_p = 5MA$, $< \beta >= 3.9\%$, $\beta_{pol} = 0.78$, $a/R = 0.36$, $\kappa = 1.63$. Note that $f = 400kHz$ corresponds to a normalized frequency $R_0\omega/v_{A0} = 1$.

Fig.2. Contour plots of the real part of the binormal component of the wave electric field, $Re(E_b)$, of the $n = 1$ TAE modes corresponding to the peaks labelled "a" and "b" in Fig.1.

Fig.3 Eigenfrequencies of the $n = 1$ TAE modes "a" and "b" versus β_{pol} for the same parameters as in Fig.1 except the $p'(\psi)$ profile which is scaled by a constant factor.

Fig.4 JET saddle coils resistive coupling (top) and compressibility (ratio of amplitudes $B_{\|}/B_{\perp}$)(bottom) of the $n = 1$ TAE mode "b" versus β_{pol} for the same parameters as in Fig.1 except the $p'(\psi)$ profile which is scaled by a constant factor.

Fig.5 Radial profiles of the wave-particle DKE power transfers to electrons (continuous line), bulk ions (open symbols) and fast ions (dotted line: P_f^{homo}; filled symbols: P_f^{inhomo}) of the $n = 1$ TAE mode "a". $T_{e0} = 10keV$, $T_{i0} = 30keV$, fusion alpha particles with $n_f(s) = 10^{18} m^{-3}(1 - s^2)^{22}$, $s_{1/2} = 0.176$, $v_0/v_{A0} = 1.73$. The radial variable s is $\sqrt{\psi/\psi_s}$ where ψ_s is the poloidal flux at the plasma surface. The other parameters are the same as in Fig.1.

Fig.6 Radial profiles of v_p/v_{thi} (dashed line), v_p/v_{the} (dotted line) and $|k_{\|}|R_0$ (continuous line) of the $n = 1$ TAE mode "a" for the same parameters as in Fig.5.

Fig.7 Volume-averaged fast particle beta for marginal stability, $< \beta_f >_{cr}$, of the $n = 1$

TAE mode "a" versus alpha particle profile half-width $s_{1/2}$, for various ion temperatures T_{i0}. The other parameters are the same as in Fig.5. (The mode is stable below the curves, unstable above).

Fig.8 Volume-averaged fast particle beta for marginal stability, $< \beta_f >_{cr}$, of the $n = 1$ TAE mode "a" versus fast ion density profile half-width $s_{1/2}$, for various values of v_0/v_{A0} and fixed plasma bulk beta of 3% and $T_{i0} = 1.25T_{e0}$. v_0/v_{A0} is changed by varying the bulk density n_0 and the temperatures T_{i0} and T_{e0} as $1/n_0$, keeping B_0 constant. $R_0 = 1.8m$, $B_0 = 0.74T$, deuterium fast particles injected at $75keV$.

Fig.9 $< \beta_f >_{cr}$ of the $n = 1$ TAE mode "a" versus v_0/v_{A0} for various values of fast ion density profile half-width $s_{1/2}$ for $\beta = 3\%$. Other parameters: same as in Fig.8.

Fig.10 $< \beta_f >_{cr}$ of the $n = 1$ TAE mode "a" versus v_0/v_{A0} for various values of plasma bulk β for a fixed fast ion density profile half-width $s_{1/2} = 0.4$. Other parameters: same as in Fig.8.

Fig.11 $< \beta_f >_{cr}$ of the $n = 1$ TAE mode "b" versus fast ion density profile half-width $s_{1/2}$ for various values of v_0/v_{A0} and fixed plasma bulk beta of 3%. Other parameters: same as in Fig.8.

Fig.12 $< \beta_f >_{cr}$ of the $n = 1$ TAE mode "b" versus v_0/v_{A0} for various values of $s_{1/2}$. Other parameters: same as in Fig.8.

Fig.13 $< \beta_f >_{cr}$ of the $n = 1$ TAE mode "b" versus v_0/v_{A0} for various values of plasma bulk β for a fixed fast ion density profile half-width $s_{1/2} = 0.4$. Other parameters: same as in Fig.8.

Fig.14. Contour plot of the real part of the binormal component of the wave electric field, $Re(E_b)$, of the $n = 2$ TAE corresponding to the peak labelled "C" in Fig.1.

Fig.15 $< \beta_f >_{cr}$ of the $n = 2$ TAE shown in Fig.14 versus the fast ion density profile half-width $s_{1/2}$, for various values of v_0/v_{A0} and fixed plasma bulk beta of 3.86%.

Other parameters: same as in Fig.8.

Fig.16 $< \beta_f >_{cr}$ of the $n = 2$ TAE shown in Fig.14 versus v_0/v_{A0} for various values of $s_{1/2}$ and fixed plasma bulk beta of 3.86%. Other parameters: same as in Fig.8.

Fig.17. Contour plot of the real part of the binormal component of the wave electric field, $Re(E_b)$, of a $n = 3$ TAE.

Fig.18 $< \beta_f >_{cr}$ of the $n = 3$ TAE shown in Fig.17 versus the fast ion density profile half-width $s_{1/2}$, for various values of v_0/v_{A0} and fixed plasma bulk beta of 3.86%. Other parameters: same as in Fig.8.

Fig.19 $< \beta_f >_{cr}$ of the $n = 3$ TAE shown in Fig.17 versus v_0/v_{A0} for various values of $s_{1/2}$ and fixed plasma bulk beta of 3.86%. Other parameters: same as in Fig.8.

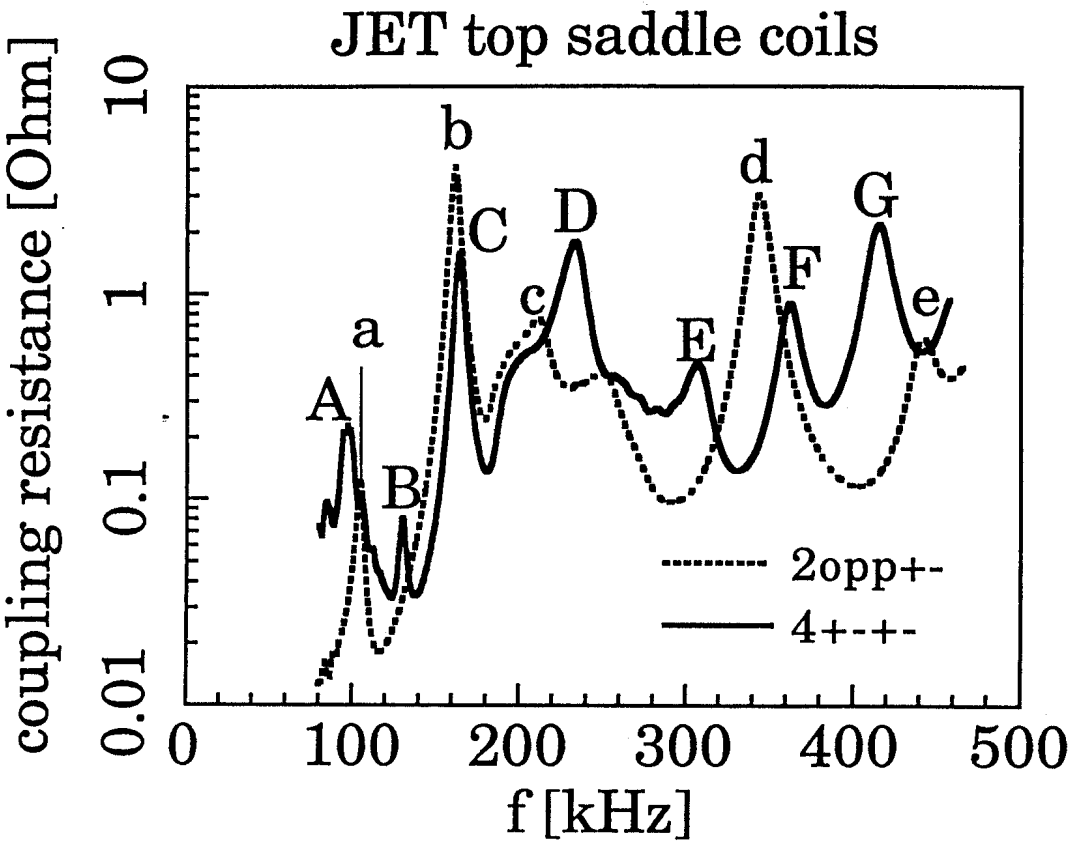
JET top saddle coils
coupling resistance [Ohm]
0.01
0.1
1
10
0
100
200
300
400
500
f [kHz]
A
a
B
b
C
c
D
E
d
F
G
e
2opp+-
4+-+-

Fig.1

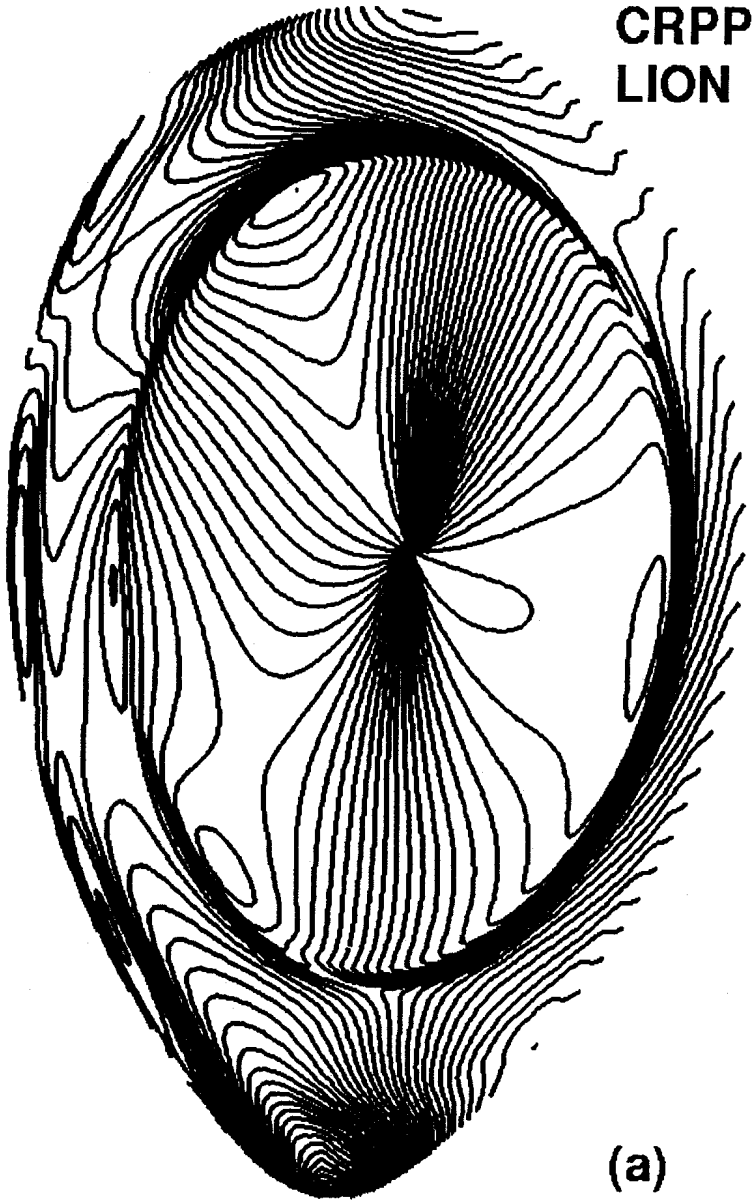

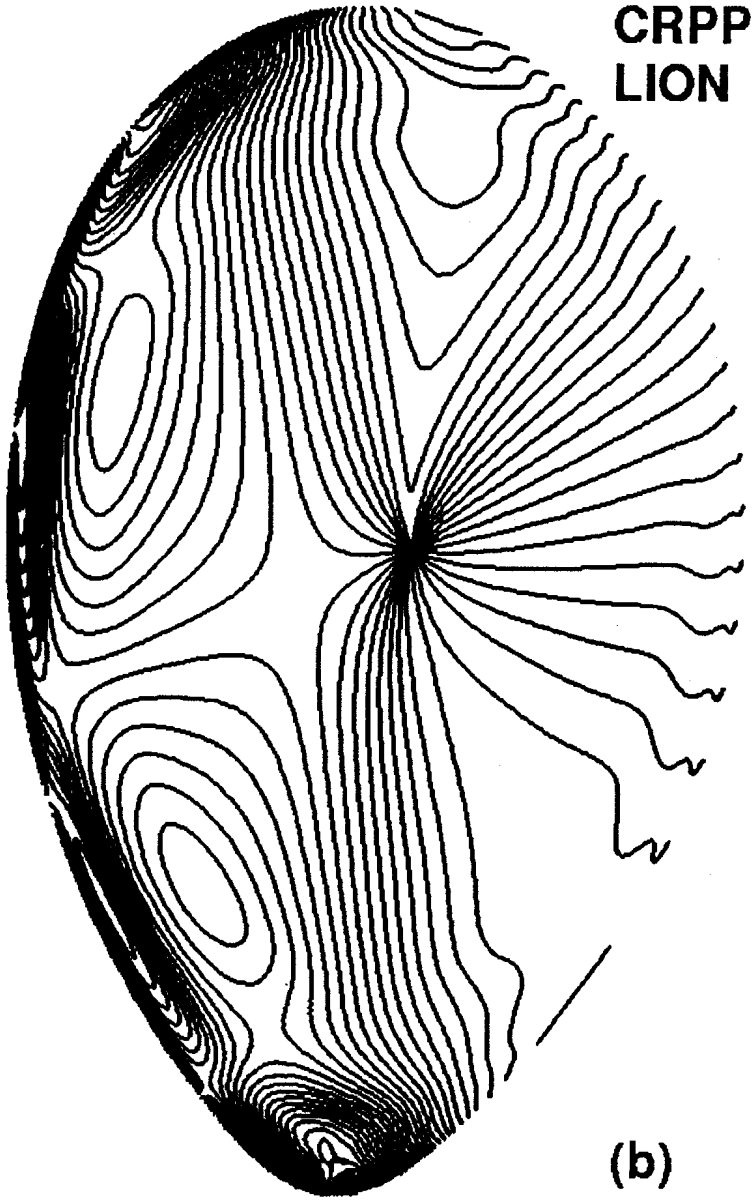

Fig.2

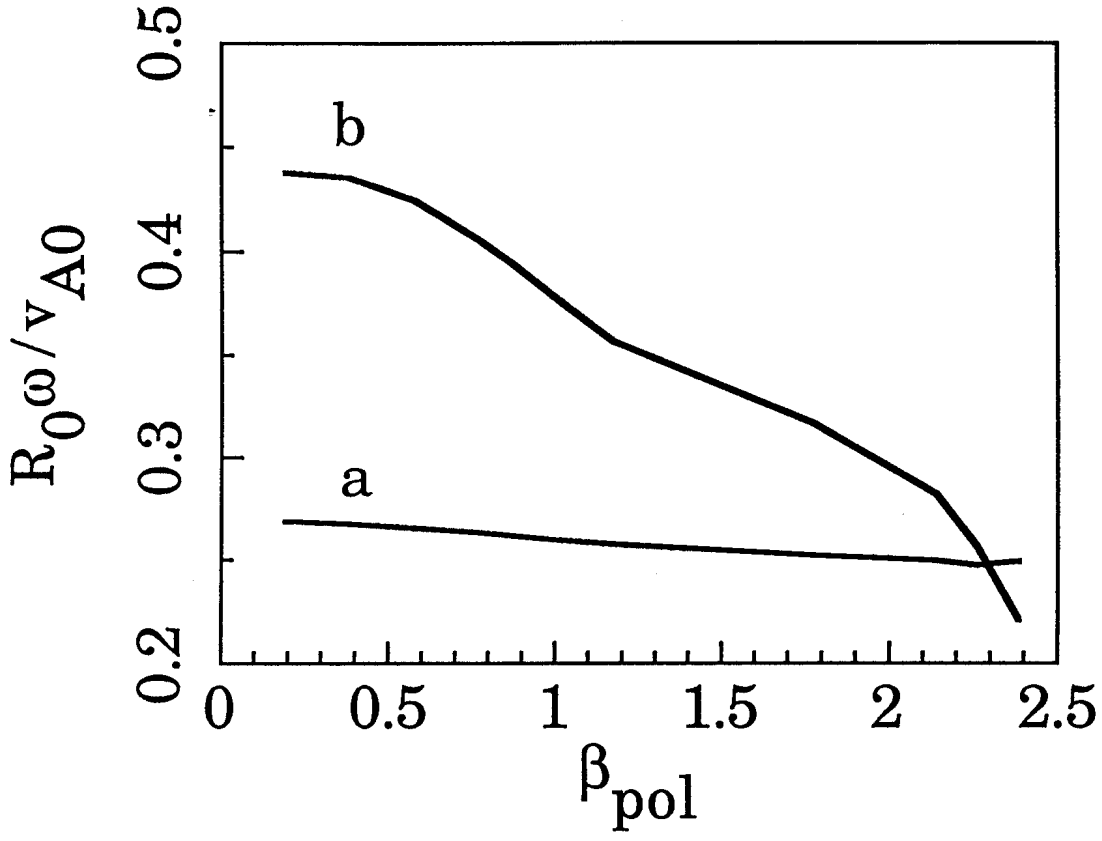

Fig.3

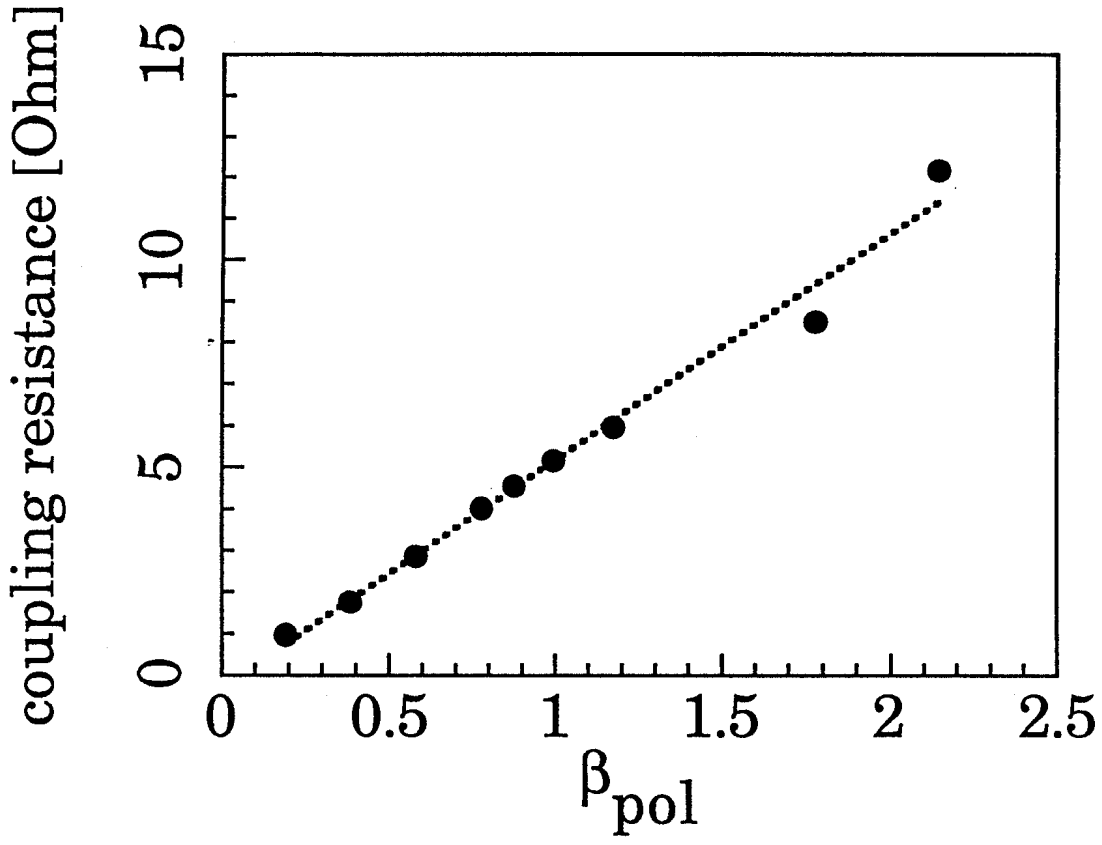
coupling resistance [Ohm]
0
5
10
15
0
0.5
1
1.5
2
2.5
β_{pol}

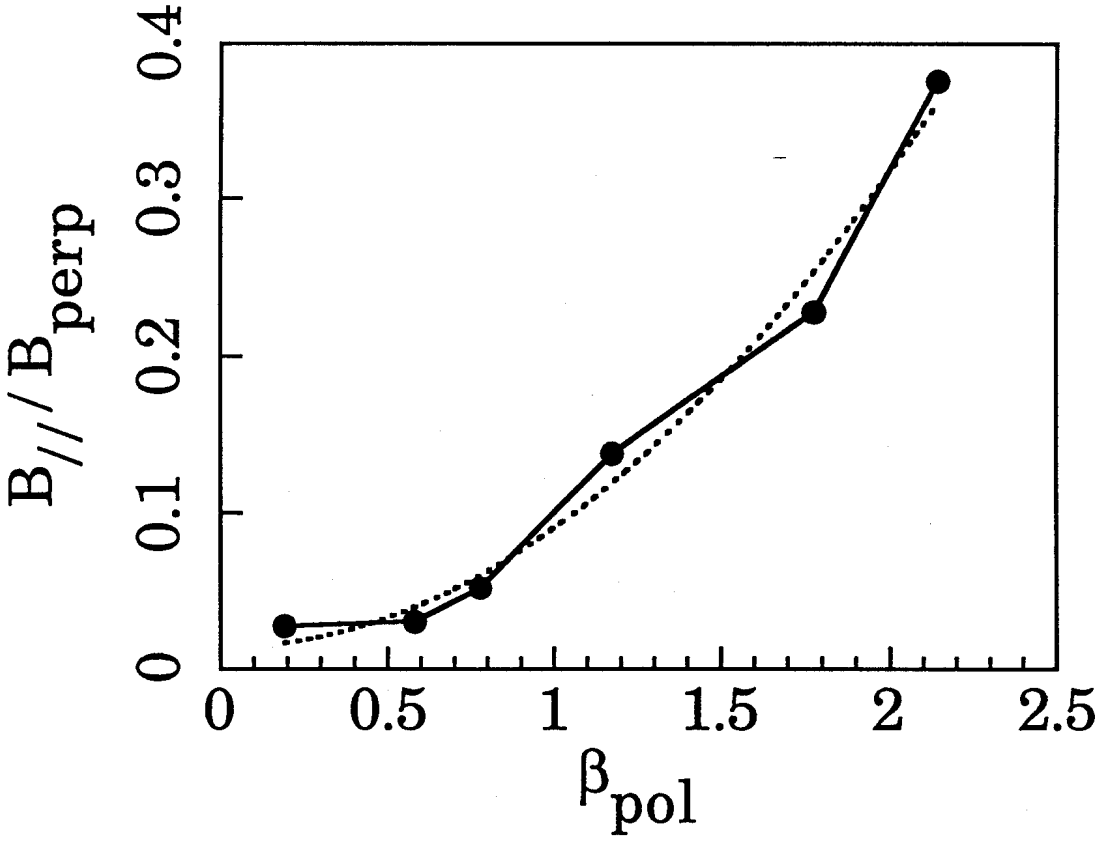
$B_{//}/B_{perp}$
0
0.1
0.2
0.3
0.4
0
0.5
1
1.5
2
2.5
β_{pol}

Fig.4

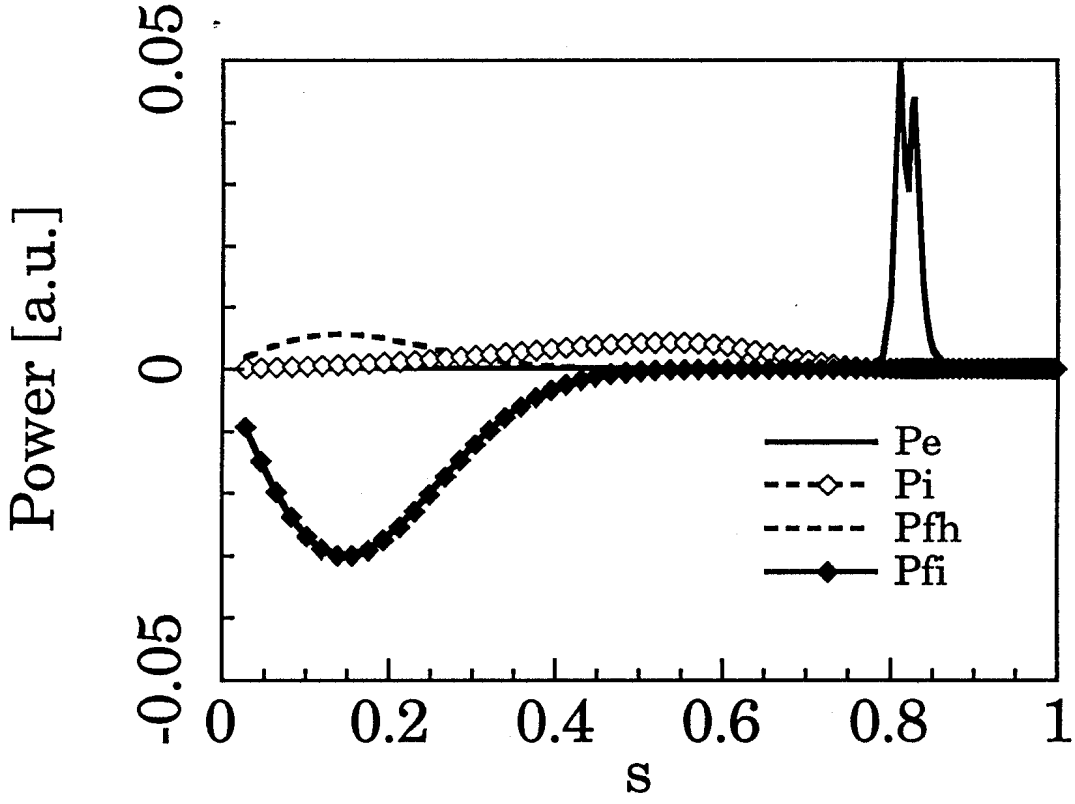

Fig.5

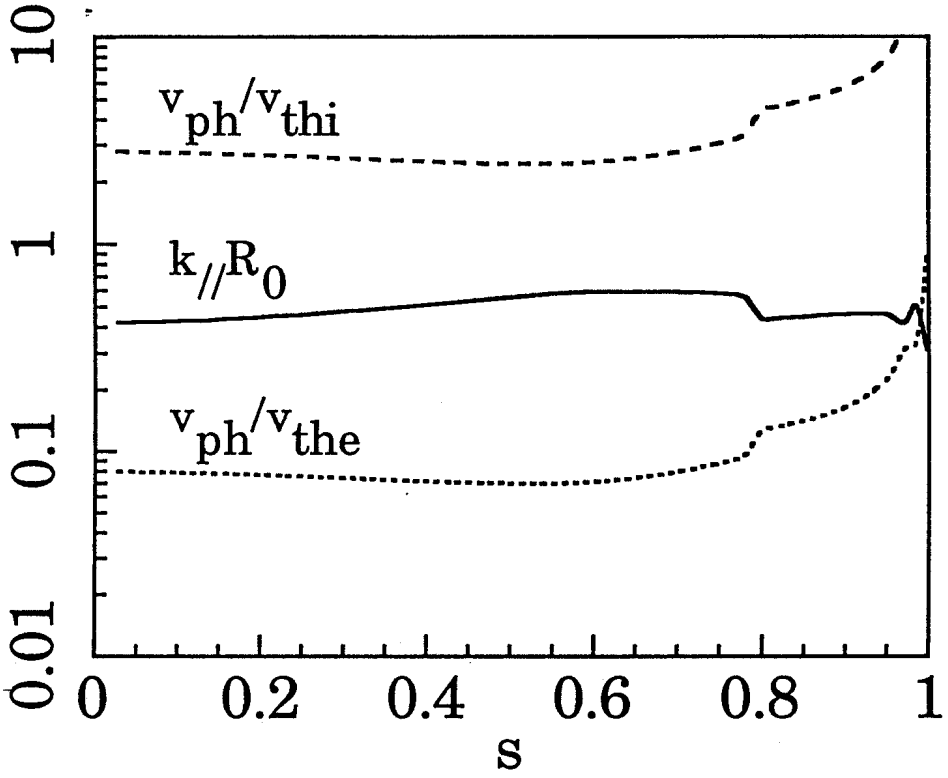

Fig.6

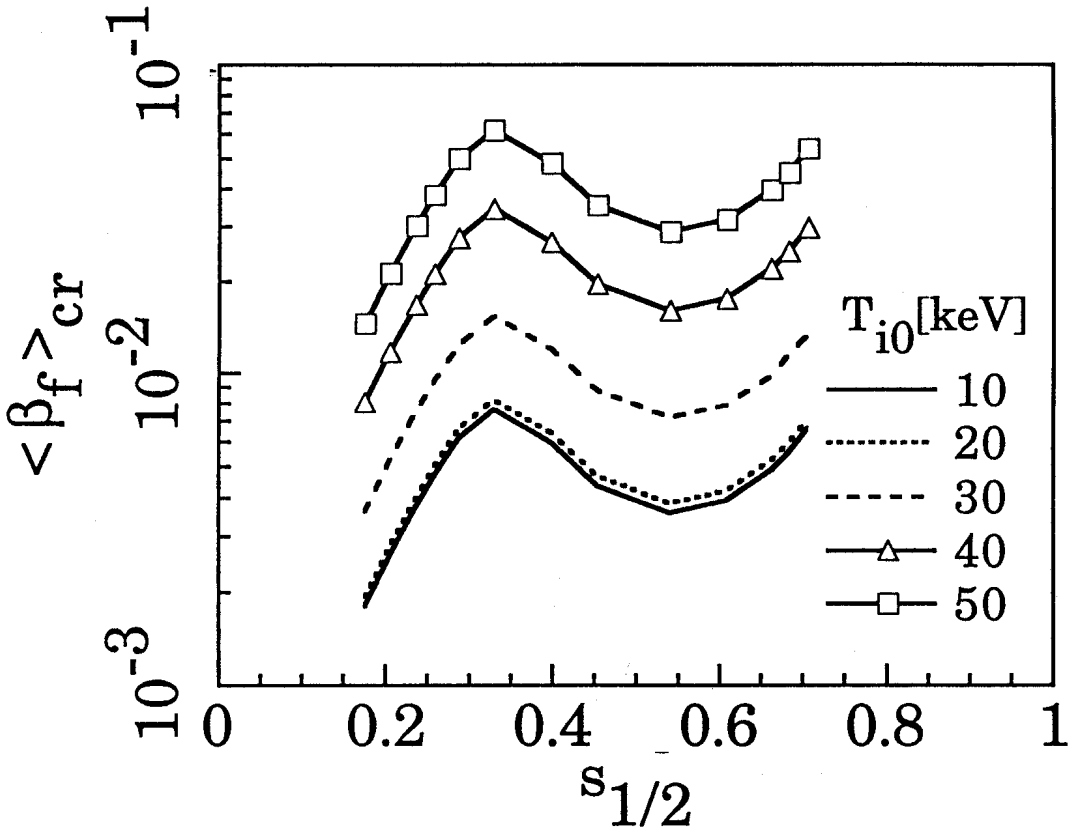

Fig.7

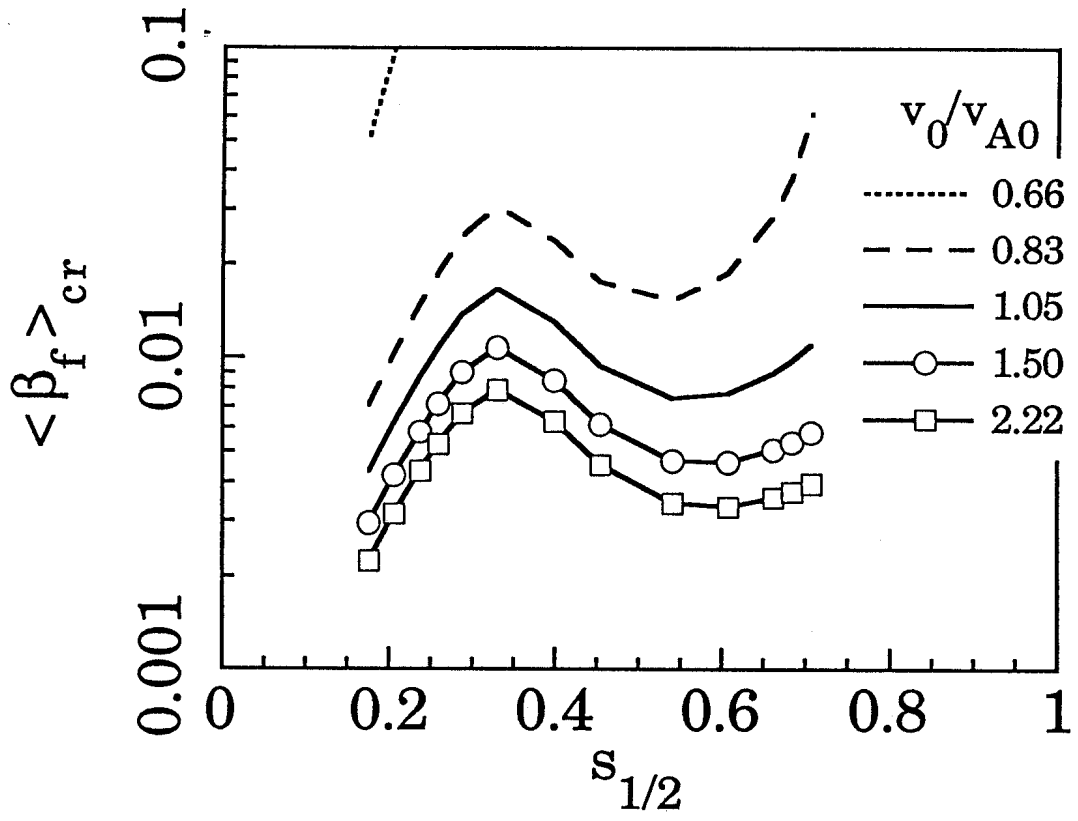

Fig.8

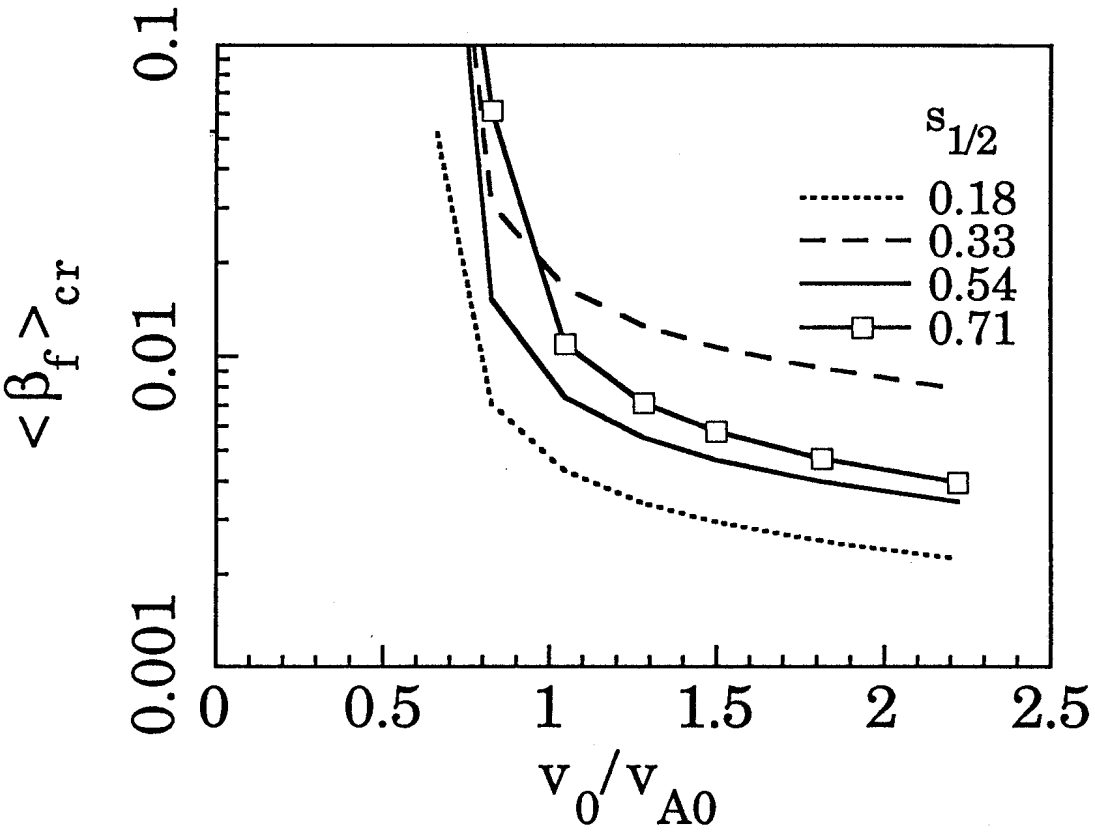

Fig.9

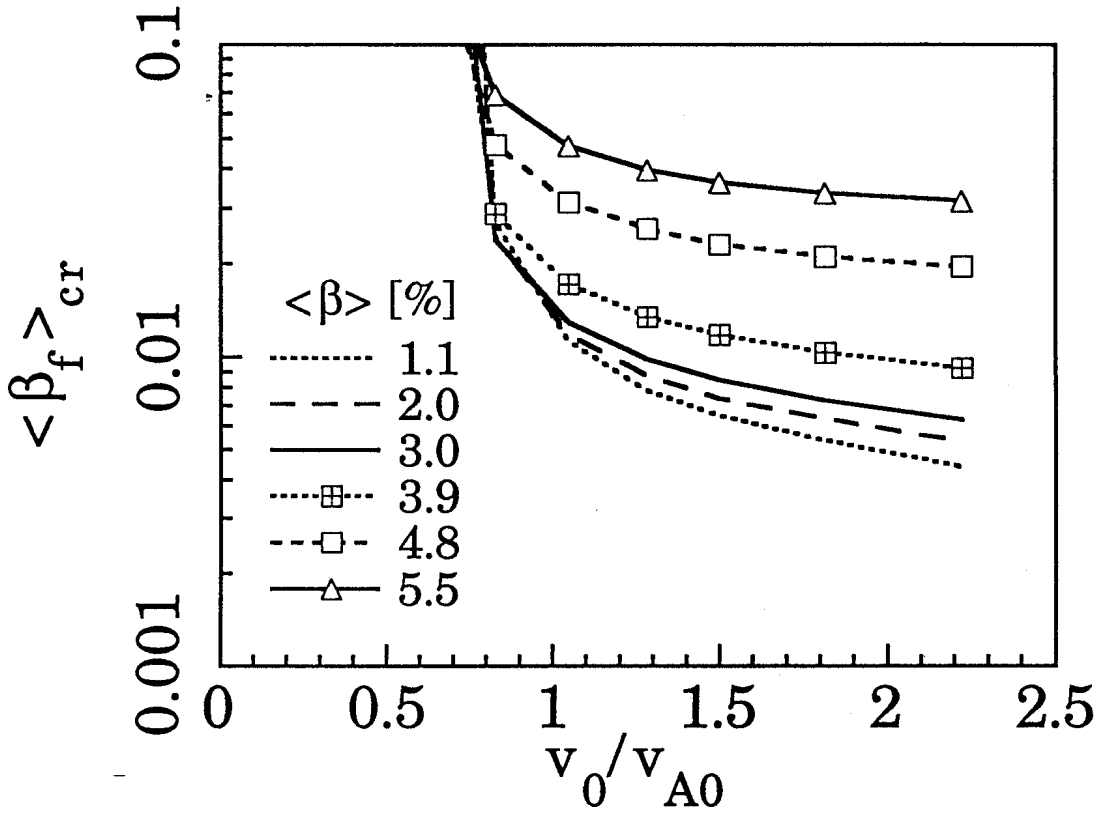

Fig.10

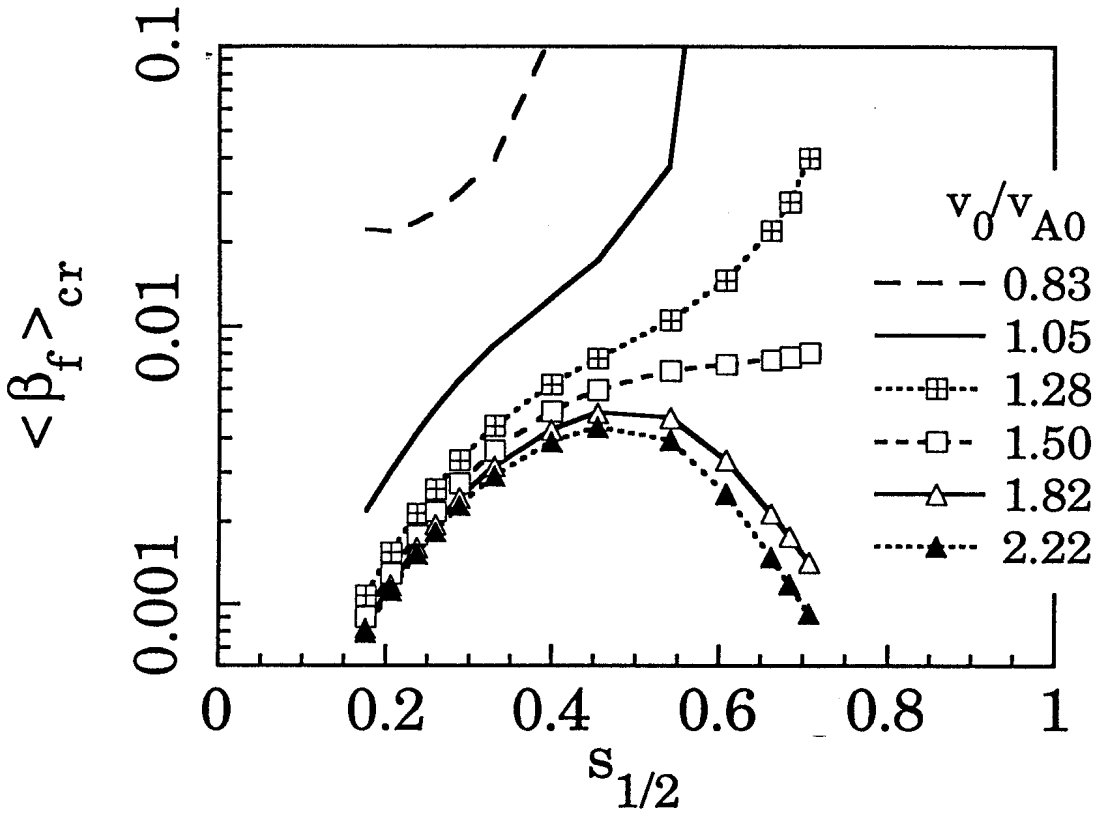
0.1
0.01
0.001
$<\beta_f>_{cr}$
0
0.2
0.4
0.6
0.8
1
$s_{1/2}$
v_0/v_{A0}
0.83
1.05
1.28
1.50
1.82
2.22

Fig.11

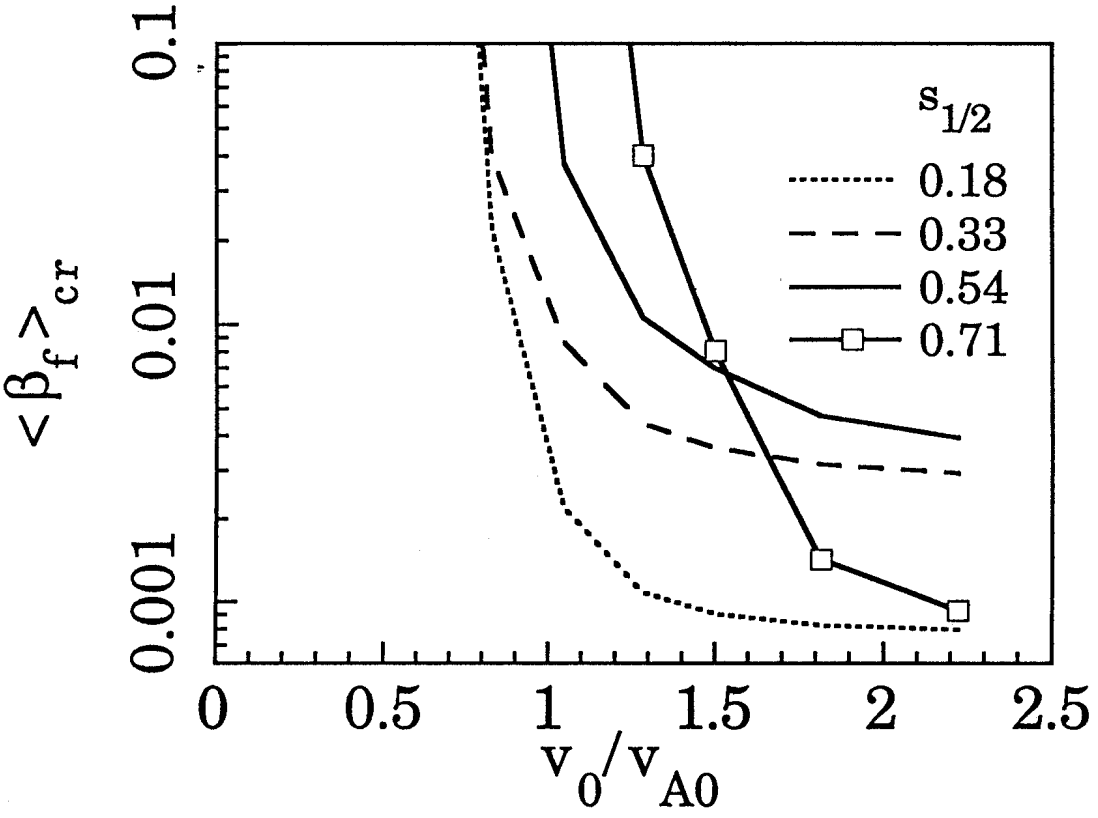

Fig.12

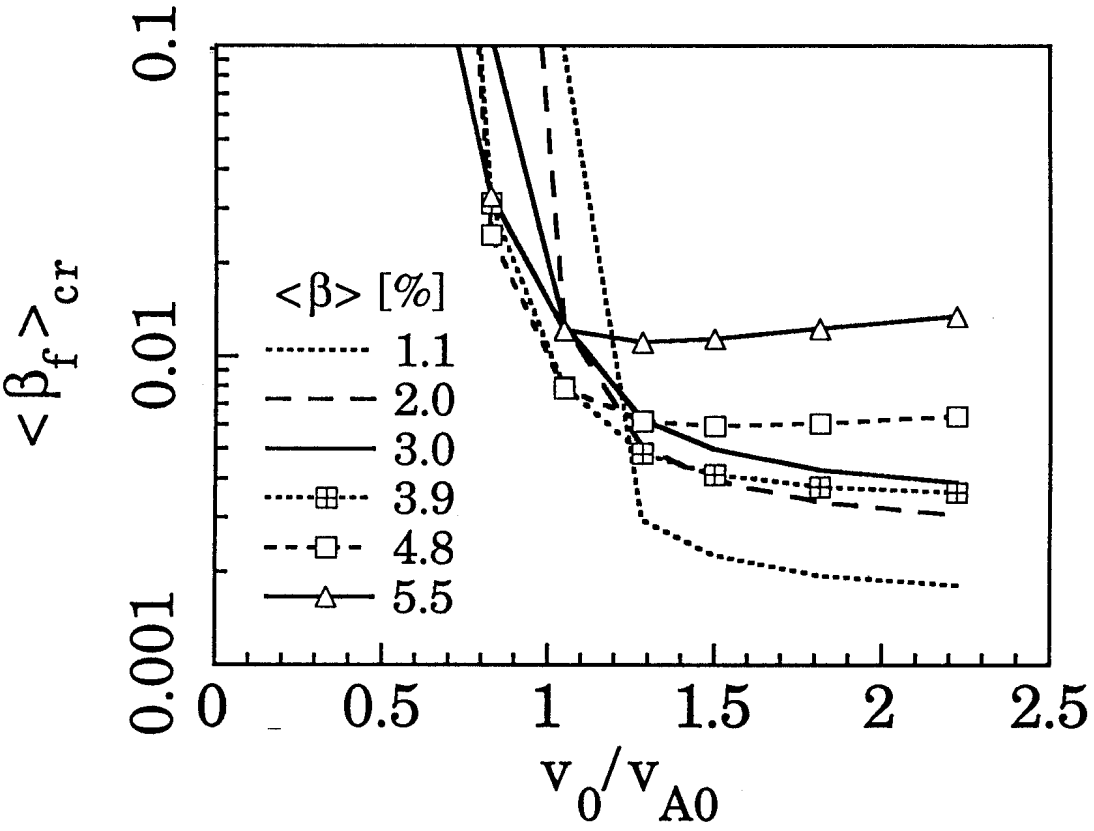

Fig.13

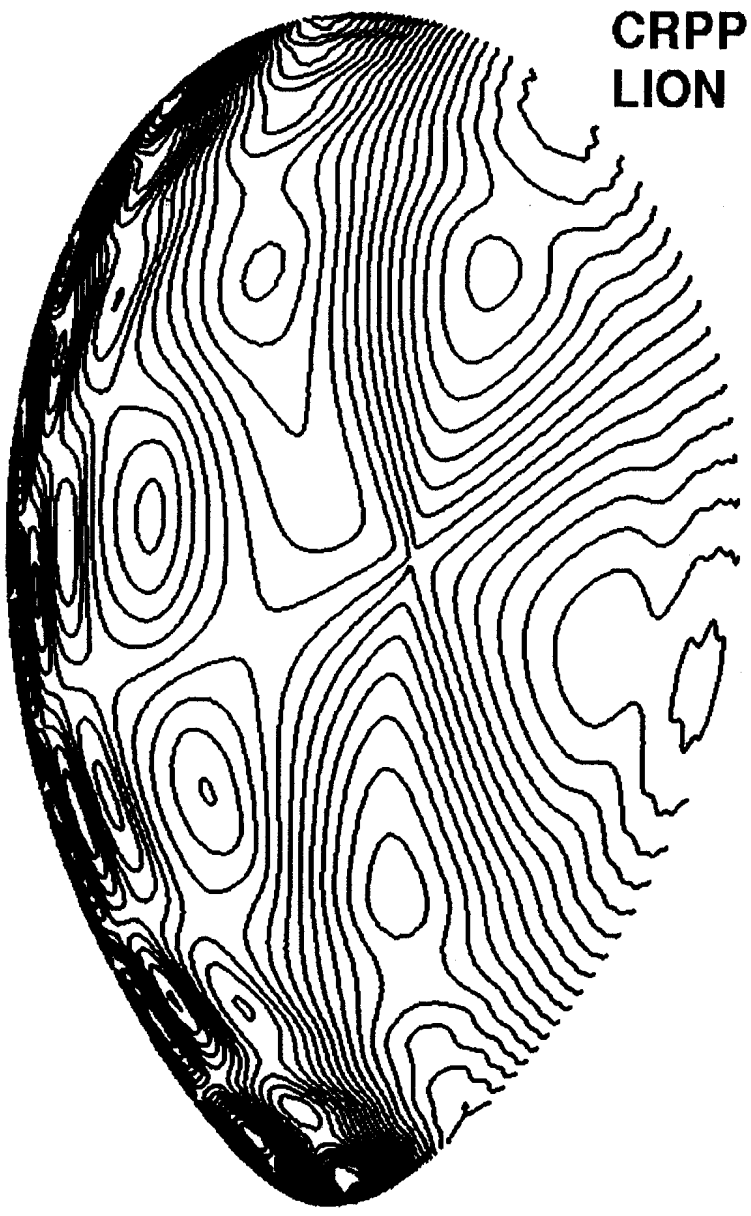

Fig.14

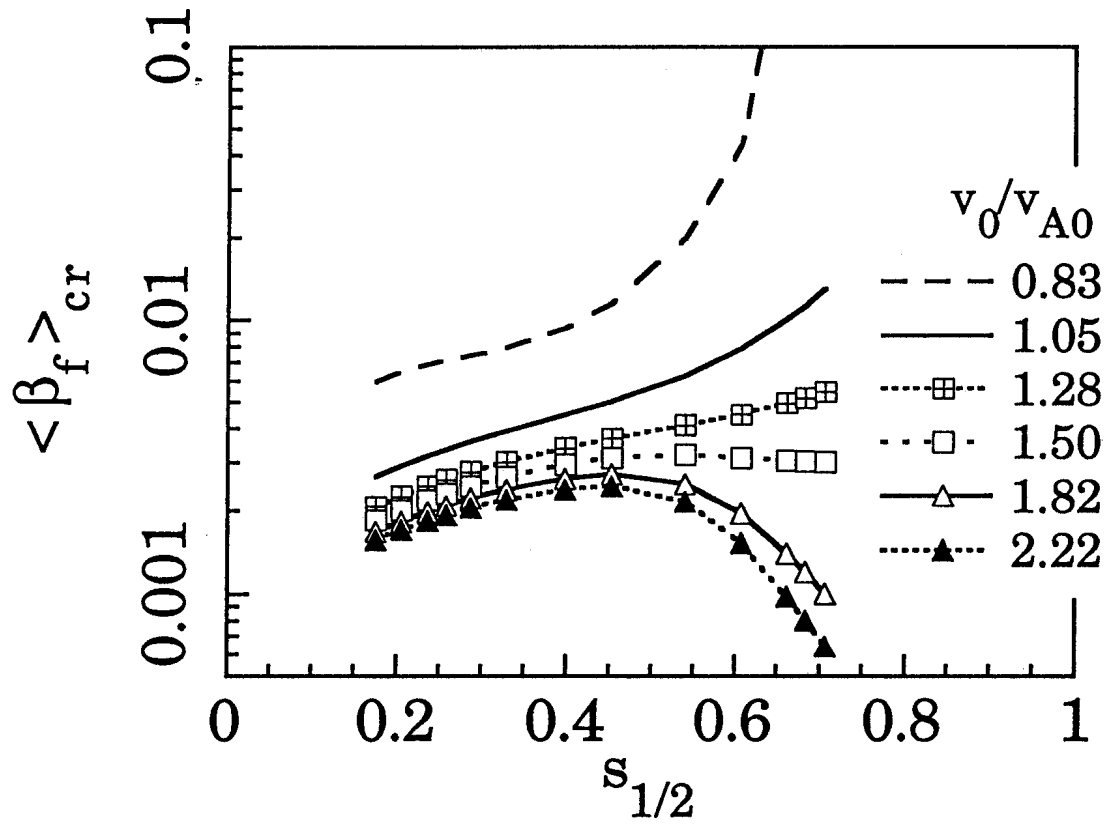
0.1
0.01
0.001
$<\beta_f>_{cr}$
0
0.2
0.4
0.6
0.8
1
$s_{1/2}$
v_0/v_{A0}
0.83
1.05
1.28
1.50
1.82
2.22

Fig.15

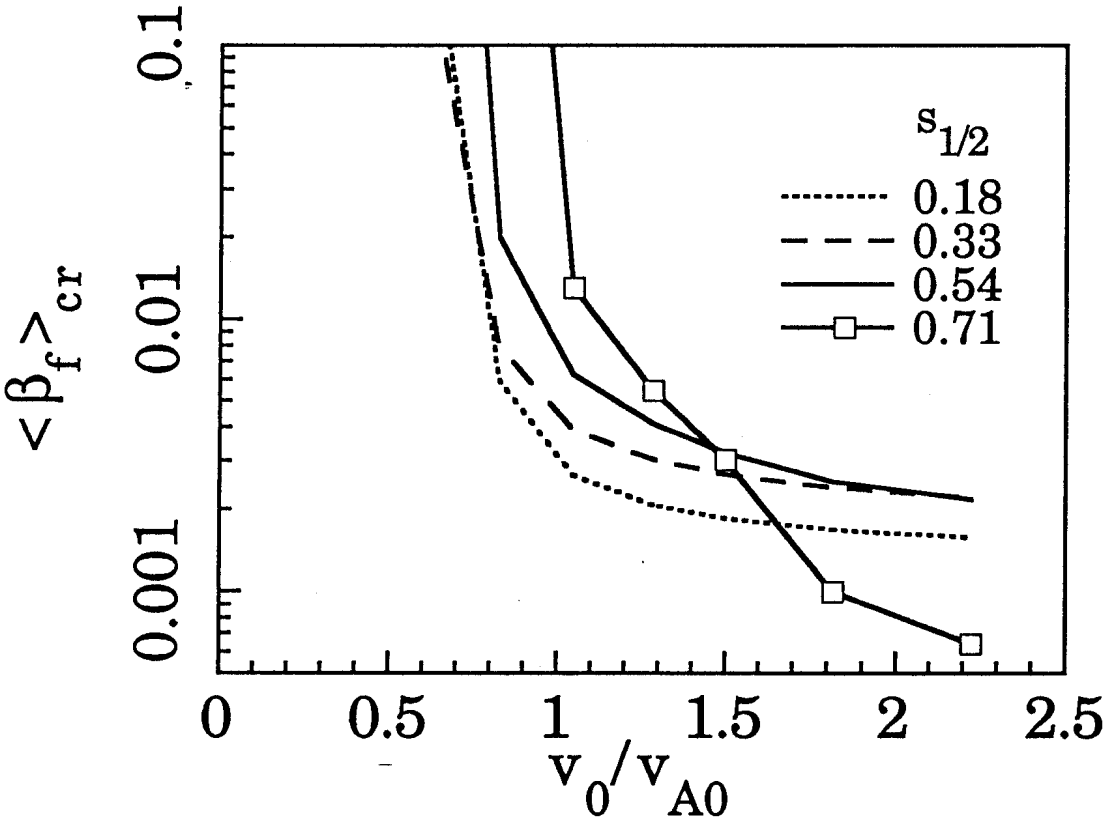

Fig.16

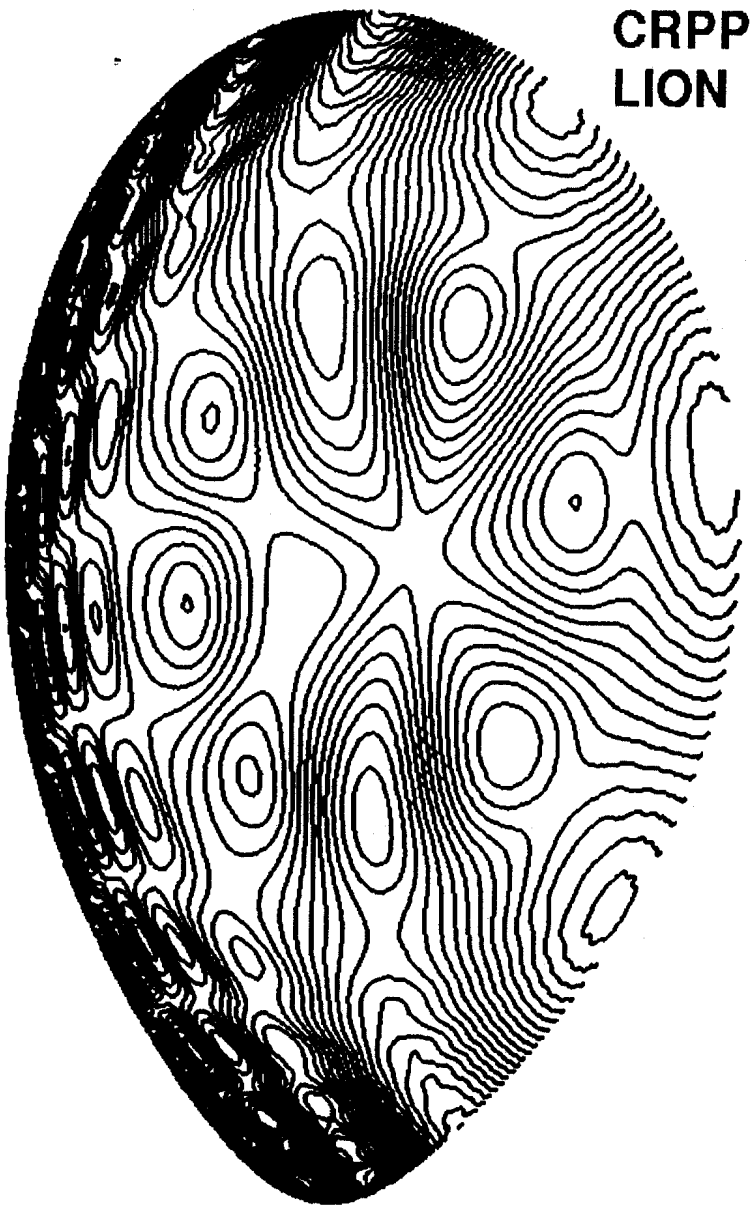

Fig.17

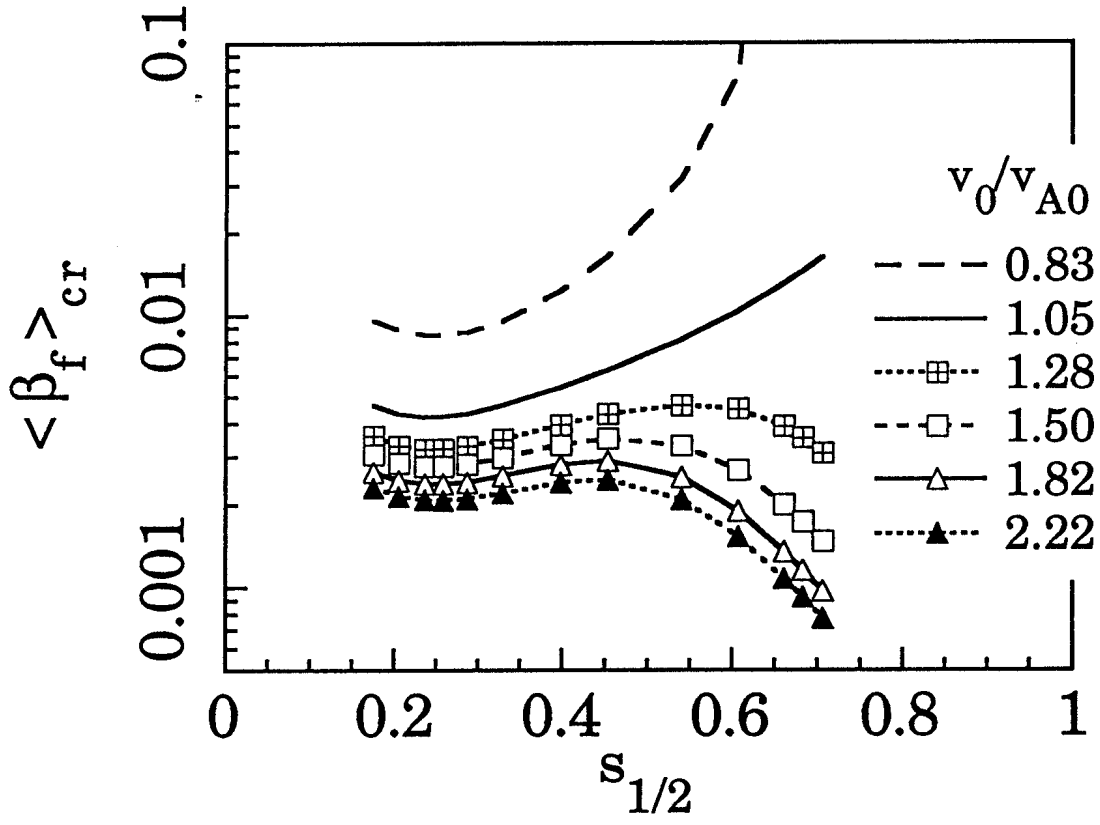
0.1
0.01
0.001
$<\beta_f>_{cr}$
v_0/v_{A0}
0.83
1.05
1.28
1.50
1.82
2.22
0
0.2
0.4
0.6
0.8
1
$s_{1/2}$

Fig.18

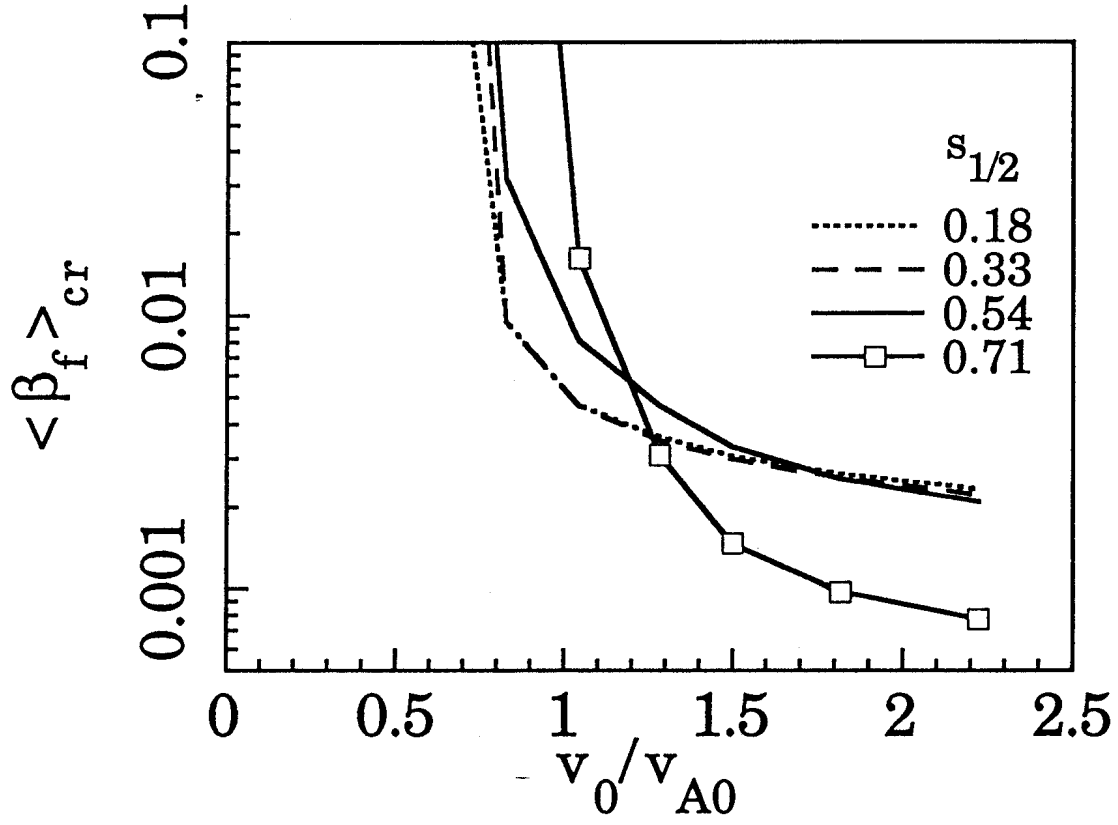

Fig.19